LEVEL SET ANALYSIS OF TWO-FLUID INTERFACIAL FLOWS

by

Aidin Sheikhi

B.S., Mechanical Engineering, Khaje Nasireddin Toosi University of Technology, 2008

Submitted to the Institute for Graduate Studies in
Science and Engineering in partial fulfillment of
the requirements for the degree of
Master of Science

Graduate Program in Mechanical Engineering
Boğaziçi University

2012

LEVEL SET ANALYSIS OF TWO-FLUID INTERFACIAL FLOWS

APPROVED BY:

Assoc. Prof. Ali Ecder (Thesis Supervisor)	.....
Assoc. Prof. Ercan Balıkçı	.....
Assist. Prof. Fatih Ecevit	.....

DATE OF APPROVAL:

To my beloved sister, Aylar Sheikhi...

ACKNOWLEDGEMENTS

First of all, I would like to thank my advisor, Assoc. Prof. Ali Ecder, who encouraged me during the whole M.S. program; I also want to thank for his continuous support, contribution, and guidance. Also, I am thankful to Assoc. Prof. Ercan Balıkçı and Assist. Prof. Fatih Ecevit for their useful guidance and opinions on my thesis. Moreover, I want to thank my professors, Prof. Akın Tezel, Assoc. Prof. Kunt Atalık, Assist. Prof. Murat Çelik, and Prof. Sabri Altıntaş, for their efforts in training and educating me.

I cannot neglect the efforts and nonstop supports of my family, my mother Amansoltan Sheikhi, my father Mohammad Sheikhi, my beloved sister Aylar Sheikhi who always trust on me and encourage me to overcome obstacles in my life; I owe every success till now to them and their compassions. Also, I want to thank my dear aunts, Azita Sheikhi and Salimeh Sheikhi, and my uncles, Kambiz sheikhi, Mahmood Sheikhi, and Taher Sheikhi whom I always feel their sympathy.

Moreover, I have valuable friends who never leave me alone with my troubles; thank you Mustafa Engin Danis, Emre Türköz, Yalın Kaptan, Erhan Turan, Uğur Türk, and Saloor Sasan.

ABSTRACT

LEVEL SET ANALYSIS OF TWO-FLUID INTERFACIAL FLOWS

In this study incompressible immiscible two-phase flows have been analyzed in two dimensions using Level Set method. Firstly, a brief explanation about other numerical methods existing in the field of modelling interfacial two-phase flows is presented. Then, Level Set methodology and its coupling with Navier-Stokes equations are introduced in detail. Discretization method used in this study is Finite Difference method and derivations of Level Set function and convective terms are done using fifth order Weighted Essentially Non-Oscillatory (WENO) scheme. In order to solve the pressure field implicitly, a projection method is applied. Afterwards, the reliability of method is tested by making comparison with Smoothed Particle Hydrodynamic (SPH) method for different test cases such as Rayleigh-Taylor instability, rising bubble, droplet fall, bursting bubble at free surface and droplet fall onto free surface. Effects of non-dimensional parameters like Reynolds (Re) and Eotvos (Eo) numbers on the evolution of interface in two-phase flows are investigated. Lastly, dam breaking problem is considered in order to analyze the performance of Level Set method in simulating free surface flows.

ÖZET

İKİ-AKIŞKANLI ARAYÜZEY AKIŞLARININ DÜZEY KÜMESİ ANALİZİ

Bu çalışmada Düzey Kümesi metodu kullanarak iki boyutlu, sıkıştırılamayan, karışmayan, iki-fazlı akışkanların analizi yapılmıştır. İlk önce, iki fazlı arayüzey akışkanların modellemesi alanında var olan diğer sayısal yöntemlerin özet açıklaması sunulmuştur. Sonra, Düzey Kümesi metodolojisi ve onun Navier-Stokes denklemleriyle bağlaşması detaylı bir şekilde anlatılmıştır. Bu çalışmada kullanılan ayrıklaştırma metodu Sonlu Farklar metodudur. Ayrıca Düzey Kümesi fonksiyonu ve taşınım terimlerinin türetilmesi beşinci derece Ağırlıklı Ortalama Esasen Salınımsız (WENO) düzeni kullanılarak yapılmıştır. Basınç alanını zımni olarak çözebilmek için projeksiyon metodu uygulanmıştır. Daha sonra, metodun güvenilirliği Rayleigh-Taylor instabilitesi, baloncuğun yükselmesi, damlacığın düşmesi, serbest yüzey de baloncuğun patlaması ve damlacığın serbest yüzeye düşmesi gibi beş farklı test problemi ile Yumuşatılmış Parçacık Hidrodinamiği (SPH) metoduyla karşılaştırılarak sınanmıştır. Boyutsuz parametrelerin, örneğin Reynolds (Re) ve Eotvos (Eo) sayıların, iki-fazlı akışkanlardaki arayüzeyın değişimi üzerindeki etkisi incelenmiştir. Son olarak, Düzey Kümesi metodunun serbest yüzey akısların simülasyonundaki performansını analiz etmek için, baraj yıkılma problemi dikkate alınmıştır.

TABLE OF CONTENTS

ACKNOWLEDGEMENTS iv
ABSTRACT v
ÖZET vi
LIST OF FIGURES ix
LIST OF SYMBOLS xii
LIST OF ACRONYMS/ABBREVIATIONS xiv
1. INTRODUCTION 1
1.1. Motivation 1
1.2. Numerical Methods for multiphase fluid flows 1
1.2.1. Lagrangian approach 2
1.2.2. Eulerian approach 3
2. Mathematical Modeling 6
2.1. Level Set Methodology 6
2.1.1. Distance and Signed-Distance Functions 7
2.1.2. Level Set Equation 9
2.1.3. Re-Initialization 9
2.1.4. Spatial and Temporal Derivatives 10
2.1.5. ENO Schemes 10
2.1.6. Runge-Kutta Method 12
2.2. Governing Equations 13
2.2.1. Surface Tension Force Term 14
2.2.2. Continuum Surface Force approach 15
2.2.3. Smoothing 16
2.2.4. Projection method 17
2.2.5. Discretization 18
2.2.6. Derivation 19
2.2.7. Interpolation 20
2.3. Non-dimensionalization 22
2.4. Mass Conservation 22

3. Results and Discussion 23
3.1. Code Validation 23
3.2. Rayleigh-Taylor Instability 27
3.3. Rising Bubble 31
3.4. Droplet Fall 37
3.5. Bursting Bubble at the Free Surface 39
3.6. Droplet Fall onto the Free Surface 41
3.7. Dam Breaking 42
4. CONCLUSIONS 49
REFERENCES 51

LIST OF FIGURES

Figure 2.1. Implicit function $\phi(x) = x^2 - 1$. 7

Figure 2.2. Implicit function $\phi(x, y) = x^2 + y^2 - 1$. 7

Figure 2.3. Thick Interface region. 17

Figure 2.4. Staggered grid. 19

Figure 2.5. Position of variables in computational cell. 19

Figure 2.6. Third order lagrange interpolation scheme. 21

Figure 3.1. u and v velocity components and streamline for $Re = 100$. 24

Figure 3.2. u and v velocity components and streamline for $Re = 400$. 25

Figure 3.3. u and v velocity components and streamline for $Re = 1000$. 26

Figure 3.4. Rayleigh-Taylor Instability: — represent Level Set Function, ● represents high density particles and ○ represents low density particles. 28

Figure 3.5. Rayleigh-Taylor Instability without surface tension. 30

Figure 3.6. Rayleigh-Taylor Instability with small surface tension, $\sigma = 0.015$. . 31

Figure 3.7. Rising Bubble: — represent Level Set Function, ● represents high density particles and ○ represents low density particles. 32

Figure 3.8. Rising Bubble with low Eo number ($Eo = 25$ and $Re = 35$). 33

Figure 3.9. Rising Bubble with high Eo number ($Eo = 125$ and $Re = 35$). . . 34

Figure 3.10. Pinching off process in Rising Bubble, $Re = 700$ and $Eo = 500$. Computaions are based on 80×160 rectangle grid. 35

Figure 3.11. Merging of two bubbles, $Eo = 500$. 36

Figure 3.12. Rising of two bubbles without merging, $Eo = 50$. 37

Figure 3.13. Grid resolution, a) 20×40, b) 40×80, c) 80×160. 37

Figure 3.14. Mass conservation diagram for three different grids. "- -": 20×40, "-": 40×80, "$\cdots$": 80×160. 38

Figure 3.15. Droplet Fall: — represent Level Set Function, ● represents high density particles and ○ represents low density particles. 39

Figure 3.16. Bursting Bubble: — represent Level Set Function, ● represents high density particles and ○ represents low density particles. . . . 41

Figure 3.17. Bursting Bubble with jet formation in the presence of surface tension, $Eo = 300$. 42

Figure 3.18. Bursting Bubble without jet formation in the presence of surface tension, $Eo = 300$. 43

Figure 3.19. Pressure distribution at the moment of beginning of jet formation : a) Bubble is close to free surface. b) Bubble is far from free surface. 43

Figure 3.20. Droplet Fall onto a Free Surface: — represent Level Set Function, ● represents high density particles and ○ represents low density particles. 44

Figure 3.21. Dam Breaking without obstacle. 45

Figure 3.22. Dam Breaking with obstacle. 46

Figure 3.23. Pressure Field for Dam Breaking with obstacle. 47

Figure 3.24. Mass conservation diagram for Dam Breaking without obstacle case. 47

Figure 3.25. Mass conservation diagram for Dam Breaking with obstacle case. . 48

LIST OF SYMBOLS

A	Amplitude
C	Volume Fraction Function
Eo	Eotvos Number
F_n	Speed Function Normal to the Interface
$\vec{g}$	gravity
H	Heaviside Function
L	Characteristic Length
$\vec{n}$	Normal Vector
P	Pressure
Re	Reynolds Number
S	Viscous Stress Tensor
t	Time
$\bar{t}$	Dimensionless Time
u	Velocity in X-direction
v	Velocity in Y-direction
V	Characteristic Velocity
V_n	Velocity Normal to the Interface
Γ_f	Interface
δ	Delta Dirac Function
ϵ	Smoothing Lenght
κ	Curvature
λ	Wave Length
μ	Viscosity
$\bar{\mu}$	Dimensionless Viscosity
ρ	Density
$\bar{\rho}$	Dimensionless Density
σ	Surface Tension Coefficient

σ_c	Critical Surface Tension Coefficient
τ	Artificial Time
ϕ	Level Set Function
ω	Frequency
Ω	Computational Domain

LIST OF ACRONYMS/ABBREVIATIONS

CSF	Continuum Surface Force
ISPH	Incompressible Smoothed Particle Hydrodynamic
LSM	Level Set Method
MAC	Marker and Cell
PIC	Particle in Cell
PLIC	Piece wise Linear Interface Calculation
SMAC	Simplified Marker and Cell
SLIC	Simplified Linear Interface Calculation
SPH	Smoothed Particle Hydrodynamic
VOF	Volume of Fluid
WSPH	Weakly Compressible Smoothed Particle Hydrodynamic

1. INTRODUCTION

In this section, at first, motivation of this study is brought in order to make clear the importance of analyzing multiphase flows numerically. Then, a brief history of numerical techniques developed for interfacial multiphase flows is presented. At last, mathematical modeling which includes Level set methodology, governing equations, and derivation approximations is discussed in details.

1.1. Motivation

Movement of clouds in the air, boiling of water in kettle, melting of the ice, fuel combustion in engine, boiling of water in reactors, die-casting of metals, solidification process in metallurgy and many other phenomena are just few examples of multiphase flows that happen in our daily lives and also in many important engineering and industrial applications. Therefore, analyzing of such these flows have a great importance. There are two alternatives, experimental and numerical analysis. Although experimental analysis give more realistic, accurate and reliable results, high costs of preparing experimental setups and time consuming experiments make less accurate but faster and more economical numerical methods preferable for many researchers in this field.

1.2. Numerical Methods for multiphase fluid flows

In all multiphase flow examples mentioned earlier, two or more different phases have been separated by discrete interfaces. In order to define material properties for each phase in the flow field, it is required to create an interface, separating different phase fields, and follow its evolution during the whole simulation. There are several numerical techniques to treat the multiphase flows, which can be categorized into two groups, Lagrangian and Eulerian approaches. While particles are used to track the interface in Lagrangian methods (interface tracking), scalar functions are used to capture the interface in Eulerian methods (interface capturing).

1.2.1. Lagrangian approach

The earliest example of Lagrangian methods was the Particle-in-Cell (PIC) method developed by F.Harlow [1], who developed the original PIC code at Los Alamos laboratories in 1958, in which mass particles are defined to carry fluid information such as mass, position, density, etc. Although PIC showed a great success in handling discontinuities over the interface, results were not satisfactory due to numerical diffusions.

Later, in 1965, Harlow and Welch developed the first Marker and Cell (MAC) method [2] for free surface flows. In MAC method both Lagrangian particles and Eulerian staggered grid using finite difference schemes are utilized. Free surface visualization was provided by virtual Lagrangian particles moving cell by cell via velocity field such that the cell contains particles are assumed to contain fluid inside. More optimizations in this method were done by Amsden and Harlow in 1970 which results in simplified MAC method (SMAC) [3].

However, there are the difficulties associated with PIC and MAC methods. For instance, increasing the number of marker particles makes these methods computationally expensive. In addition, it usually becomes hard to manage the particles (addition or deletion) when the interface experiences topological changes such as merging or pinching off. Attempts to cure these problems ended in a new method, called Front Tracking method, in which a set of connected points are used to represent the moving interface. In order to calculate the evolution of each fluid across the interface, a secondary irregular grid is employed in the vicinity of the front which moves with the interface. Different application areas for this method reflected in the works done by Glimm [4], Moretti [5], Peskin [6], Fauci [7], Fogelson [8],Trygvason [9], [10], and Unverdi [11]. Although Front Tracking method increases accuracy in capturing the interface and discontinuities across the interface, difficulties in calculation of the surface tension and implementation of general cases (e.g. three dimensional problems) and high computational efforts make this method less favourable.

Another Lagrangian method is Smoothed Particle Hydrodynamics (SPH), originally invented by Lucy [12] and Gingold and Monaghan [13] in 1977 to simulate astrophysical problems. Later on, SPH is used in a wide range of area such as Fluid Mechanics, Solid Mechanics, high velocity impact problems, film and computer game industry. SPH is a fully meshless method which uses computational particles in order to define a continuum. Any function at any point can be calculated according to its neighbor particles. Gaussian like kernel functions are used to evaluate the weight of each neighbor particle. Since particles are used in SPH, pressure can be calculated as a function of density using an equation of state in Fluid Mechanics simulation. For incompressible flows, small density variation is usually assumed and equation of state similar to Tait's equation of state is used. This approach is known as "Weakly Compressible SPH (WCSPH)" [14]. On the other hand, incompressibility can also be enforced using Conservation of Mass law and pressure can be obtained from a projection method [15].

1.2.2. Eulerian approach

While in Lagrangian approach particles are used to track the interface, scalar functions are defined to capture the moving interface in Eulerian techniques. One of the earliest methods in this area is Volume of Fluid (VOF) method which was first developed by Hirt and Nichols [16] in 1981. The idea of VOF is based on assuming a volume fraction function, C, according to the base fluid. For example, the value of C is equal to 1 in the computational cells occupied by fluid 1 and is equal to 0 in the cells occupied by fluid 2, and in the cells which are occupied partially by both fluids, the value of C varies sharply from 0 to 1. In this approach, the interface is explicitly reconstructed at each time step using Simplified Line Interface Calculation (SLIC) method of Noh and Woodward [17]. Later, modifications were done on reconstructing the interface using piece wise linear interface calculations (PLIC) by Young [18] and later by Scardoveli and Zaleski [19]. Since this method deals directly with volume fractions, satisfactory mass conservation is obtained.

Another technique in order to capture the interface in the area of Eulerian approach is Phase Field method. In this method, a very thin region is defined where the interfacial forces are distributed in a smooth way. A scalar function is defined as mass concentration which varies smoothly over the interface. In order to solve the flow field of density matched binary fluids, Navier-Stokes equations are coupled with Cahn-Hilliard equation for mass concentration which is known as model H [20]. In the cases that fluids have different densities, Lowengrub and Truskinovsky [21] proposed another Phase Field model. Scalar function used in this method has physical meaning and not only used near the interface, but in the bulk regions. Moreover, topological changes such as pinching off and merging of interface are naturally handled. However, large gradients in the phase field, which are hard to resolve computationally, is inevitable since it is required to get the interface very thin to get better results. Therefore, large number of grid points near the interface is required. To remedy this situation, recent developments were achieved by Karma [22] and Rappel [22].

Another Eulerian technique that captures the interface evolution is Level Set Method (LSM) which is recently become so popular. LSM was first introduced by Sethian and Osher [23]. Their effort in developing Level Set method was resulted in two valuable reference books, "Level Set Methods and Fast Marching Methods" [24] and "Level set methods and dynamic implicit surfaces" [25], which was referred by many authors in this field. The basic idea of LSM is to use a continuous and scalar distance function called Level Set function and evolve Level Set function implicitly by a velocity field which can be a function of external velocity field, interface curvature, and the geometry of the problem. The zero isocontour of Level Set function represents the interface itself, the negative isocontours stand for inside region, and the positive values belong to region outside the interface.

There is a vast variety of application areas in LSM such as Image Processing [26–28], Material Science [29–31] and Fluid Dynamics [32–35]. One of the outstanding characteristics of this method is its easy implementation.

There is no need to reconstruct the interface explicitly at each time step and topological changes are handled automatically by retaining the signed distance feature of this level set function. Moreover, geometric informations such as normal and curvature of the interface can be calculated easily whenever its required from the level set function. All these superiorities made us prefer LSM among other Eulerian techniques. The method will be introduced in detail in Section 2.1.

2. Mathematical Modeling

In this chapter, the concept of the Level Set method used in modeling incompressible immiscible two-phase flows and the governing equations is introduced. Firstly, a Level Set function and its properties are introduced. Then, advection equation for Level Set function, mathematical operators, and numerical techniques are presented. Morover, the governing Navier-Stokes equations for incompressible fluid flows, solution approaches, and coupling of Level Set with Navier-Stokes equations are discussed.

2.1. Level Set Methodology

In many applications, such as Material Science, Computer Graphics, Fluid dynamics, there are interfaces which seperate two or more regions or phases from each other. In order to represent the interface and its evolution, a scalar function in a higher dimension is defined implicitly, which its zero iso contour represents the interface and iso contours with negative and possitive values represent inside and outside regions respectively. This function is called Level Set function, $\phi(\vec{x}, t)$.

For instance, consider a line in one dimension which is seperated in three parts, $(-\infty, -1)$, $(-1, 1)$, and $(1, \infty)$ by points $x = 1$ and $x = -1$. We define $(-1, 1)$ as the inside and $(-\infty, -1) \cup (1, \infty)$ as the outside regions. The interface, points $x = 1$ and $x = -1$, is implicitly defined by some isocontour functions, for example $\phi(x) = x^2 - 1$ as shown in Figure 2.1.

Similarly, in two dimensions, consider a circle of radius 1, $\phi(x, y) = x^2 + y^2 - 1$, which seperates the domain into interior and exterior regions. Here, the interface is represented as a zero iso contour, $\phi(x, y) = 0$, while $\phi(x, y) < 0$ and $\phi(x, y) > 0$ represent interior and exterior regions respectively. See Figure 2.2.

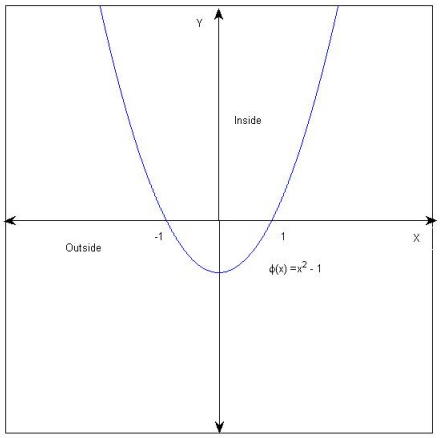


Figure 2.1. Implicit function $\phi(x) = x^2 - 1$.

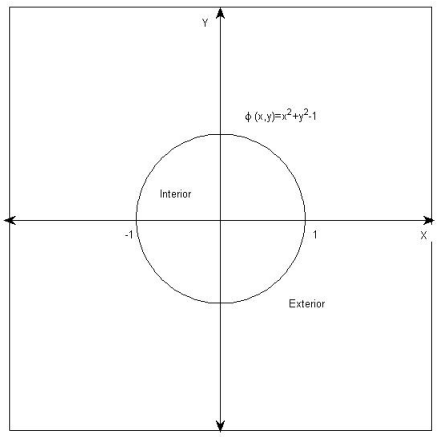


Figure 2.2. Implicit function $\phi(x, y) = x^2 + y^2 - 1$.

2.1.1. Distance and Signed-Distance Functions

In LS method, the Level Set function, $\phi(\vec{x}, t)$, is set to be a distance function, $\phi(\vec{x}, t) = d(\vec{x}, t) = min(|\vec{x} - \vec{x_I}|)$, where $\vec{x_I}$ shows the position of points on the interface and $d(\vec{x}, t)$ determines the distance of other points to the nearest points on the interface,

i.e, $d(\vec{x},t) = \sqrt{(x-x_I)^2+(y-y_I)^2+(z-z_I)^2}$. Now, $\nabla d(\vec{x},t)$ can be calculated as

$$\nabla d(\vec{x},t) = \begin{bmatrix} \frac{d}{dx}d(x) \\ \frac{d}{dy}d(y) \\ \frac{d}{dz}d(z) \end{bmatrix} = \begin{bmatrix} \frac{1}{2}\frac{2(x-x_I)}{\sqrt{(x-x_I)^2+(y-y_I)^2+(z-z_I)^2}} \\ \frac{1}{2}\frac{2(y-y_I)}{\sqrt{(x-x_I)^2+(y-y_I)^2+(z-z_I)^2}} \\ \frac{1}{2}\frac{2(x-x_I)}{\sqrt{(x-x_I)^2+(y-y_I)^2+(z-z_I)^2}} \end{bmatrix} \tag{2.1}$$

Consequently,

$$\begin{aligned} |\nabla d(\vec{x},t)| = (&\frac{(x-x_I)^2}{(x-x_I)^2+(y-y_I)^2+(z-z_I)^2} \\ &+\frac{(y-y_I)^2}{(x-x_I)^2+(y-y_I)^2+(z-z_I)^2} \\ &+\frac{(x-x_I)^2}{(x-x_I)^2+(y-y_I)^2+(z-z_I)^2}) = 1 \end{aligned}$$

Since positive and negative isocontours represent interior and exterior regions, Level Set function, $\phi(\vec{x},t)$, is defined as

$$\phi(\vec{x},t) = \begin{cases} d(\vec{x},t) & \text{Exterior} \\ 0 & \text{Interface} \\ -d(\vec{x},t) & \text{Interior} \end{cases} \tag{2.2}$$

While $\phi(\vec{x},t) = d(\vec{x},t)$, $|\nabla\phi(\vec{x},t)| = 1$. This Level Set function is called signed distance function.

Geometric properties of the interface such as normal vector, $\vec{n}$, and curvature, κ, can be easily calculated using Level Set function, ϕ, i.e,

$$\vec{n} = \frac{\nabla\phi}{|\nabla\phi|} \qquad \text{and} \qquad \kappa = \nabla\cdot\vec{n} \tag{2.3}$$

2.1.2. Level Set Equation

In order to capture the interface evolution, movement of the Level Set function, $\phi(\vec{x}, t)$, should be followed via advection equation of $\phi(\vec{x}, t)$ which is also known as Level Set equation.

$$\frac{\partial \phi}{\partial t} + F_n |\nabla \phi| = 0 \tag{2.4}$$

where F_n is a speed function normal to the interface and it differs depending on many factors such as the geometry of the problem, local curvature (κ), underlying velocity field that transports the interface, etc. For example, in the case of two-phase incompressible fluid flows, the speed function is the vlocity field solved from Navier-Stokes equations. Therefore, F_n in Equation 2.4 is turned to be $\vec{V_n} = \vec{V} \cdot \vec{N}$ and since $\vec{N} = \frac{\nabla \phi}{|\nabla \phi|}$, Level Set equation is changed to

$$\frac{\partial \phi}{\partial t} + \vec{V} \cdot \nabla \phi = 0 \tag{2.5}$$

2.1.3. Re-Initialization

As level Set function is evolved, it is not remained signed distance. To avoid this situation, a so called re-initialization step in which the current level-set function is replaced by a smoother, less distorted function which has the same zero level-set, must be performed. The procedure is as follows:

$$d_\tau + sign(\phi)(|\nabla d| - 1) = 0 \tag{2.6}$$

With initial value $d(\vec{x}, 0) = \phi(\vec{x})$. Where $\phi(\vec{x})$ is the level Set function calculated from Equation 2.4.

There are many variants of mollified signum function ($sign(\phi)$), one of them is

due to Sussman *et al.* [33]

$$S(\phi) = \frac{\phi}{\sqrt{(\phi)^2 + \delta x^2}} \tag{2.7}$$

Another one is due to Peng *et al.* [36]

$$S(\phi) = \frac{\phi}{\sqrt{(\phi)^2 + |\nabla\phi|^2(\delta x)^2}} \tag{2.8}$$

In this study, $sign(\phi)$ is calculated due to equation suggested by Peng. The Equation 2.6 is evolved till meet the steady state condition.

2.1.4. Spatial and Temporal Derivatives

Approximation techniques used for spatial and temporal derivations in Equations 2.6 and 2.5 are discussed in this section. In order to improve accuracy in approximated derivations, Essentially Non-Oscillatory (ENO) schemes and third order Runge-Kutta method are applied for spatial and temporal derivatives respectively. All discretizations are done in the finite difference framework in following sections.

2.1.5. ENO Schemes

Since level set methods are so sensitive to the accuracy used in discretizing the spatial derivatives, we apply robust and accurate Essentially Non Oscillatory (ENO) scheme [37] in order to calculate the convective terms of Equation 2.4 for the evolution of the interface. for example, to calculate $u\phi_x$ term in Equation 2.4, according to the direction of u ($u < 0$ or $u > 0$), we take $\phi_x = \phi_x^+$ or $\phi_x = \phi_x^-$.

To find ϕ_x^-, set

$$\upsilon_1 = \frac{\phi_{i-2} - \phi_{i-3}}{\Delta x} \quad , \quad \upsilon_2 = \frac{\phi_{i-1} - \phi_{i-2}}{\Delta x}$$

$$v_3 = \frac{\phi_i - \phi_{i-1}}{\Delta x} \qquad , \qquad v_4 = \frac{\phi_{i+1} - \phi_i}{\Delta x}$$

$$v_5 = \frac{\phi_{i+2} - \phi_{i+1}}{\Delta x}$$

and to find ϕ_x^+, set

$$v_1 = \frac{\phi_{i+3} - \phi_{i+2}}{\Delta x} \qquad , \qquad v_2 = \frac{\phi_{i+2} - \phi_{i+1}}{\Delta x}$$

$$v_3 = \frac{\phi_{i+1} - \phi_i}{\Delta x} \qquad , \qquad v_4 = \frac{\phi_i - \phi_{i-1}}{\Delta x}$$

$$v_5 = \frac{\phi_{i-1} - \phi_{i-2}}{\Delta x}$$

we use these first order derivation schemes to obtain three different polynomial approximations of $\phi_x^{\pm}$,

$$\phi_x^1 = \frac{v_1}{3} - \frac{7v_2}{6} + \frac{11v_3}{6} \tag{2.9}$$

$$\phi_x^2 = \frac{-v_2}{6} + \frac{5v_3}{6} + \frac{v_4}{3} \tag{2.10}$$

$$\phi_x^3 = \frac{v_3}{3} + \frac{5v_4}{6} - \frac{v_5}{6} \tag{2.11}$$

in this study, we applied weighted ENO scheme where a weighted convex combination of equations (2.9)-(2.11) is used. The weights ω_1, ω_2, andω_3 are calculated using an

estimate of the smoothness of each stencil given by

$$S_1 = \frac{13}{12}(v_1 - 2v_2 + v_3)^2 + \frac{1}{4}(v_1 - 4v_2 + 3v_3)^2$$
$$S_2 = \frac{13}{12}(v_2 - 2v_3 + v_4)^2 + \frac{1}{4}(v_2 - v_4)^2$$
$$S_3 = \frac{13}{12}(v_3 - 2v_4 + v_5)^2 + \frac{1}{4}(3v_3 - 4v_4 + v_5)^2$$

and the weights by

$$a_1 = \frac{1}{10}\frac{1}{(\epsilon + S_1)^2} \quad , \quad \omega_1 = \frac{a_1}{a_1 + a_2 + a_3}$$
$$a_2 = \frac{6}{10}\frac{1}{(\epsilon + S_2)^2} \quad , \quad \omega_2 = \frac{a_2}{a_1 + a_2 + a_3}$$
$$a_3 = \frac{3}{10}\frac{1}{(\epsilon + S_3)^2} \quad , \quad \omega_3 = \frac{a_3}{a_1 + a_2 + a_3}$$

in order to obtain

$$(\phi_x^{\pm})_i = \omega_1(\frac{v_1}{3} - \frac{7v_2}{6} + \frac{11v_3}{6}) + \omega_2(\frac{-v_2}{6} + \frac{5v_3}{6} + \frac{v_4}{3}) + \omega_3(\frac{v_3}{3} + \frac{5v_4}{6} - \frac{v_5}{6}) \quad (2.12)$$

note that $\epsilon = 10^{-6}$.

2.1.6. Runge-Kutta Method

In order to improve accuracy and stability, a third order Total Variation Diminishing (TVD) Runge-Kutta method is applied in Equation 2.6. If $sign(\phi)(|\nabla d| - 1)$ term in Equation 2.6 is assumed as $-L(\phi)$ and took to the right hand side of the equation, it is changed to $\phi_\tau = L(\phi)$. Now, the third order TVD Runge-Kutta method is

applied to this equation as follows

$$\phi^1 = \phi^n + \delta t L(\phi^n) \tag{2.13}$$

$$\phi^2 = \phi^n + \frac{\delta t}{4}[L(\phi^n) + L(\phi^1)] \tag{2.14}$$

$$\phi^{n+1} = \phi^n + \frac{\delta t}{6}[L(\phi^n) + 4L(\phi^2) + L(\phi^1)] \tag{2.15}$$

2.2. Governing Equations

In this study, $2-D$ fluid motion is considered. Behaviour of the fluids is governed by the incompressible Navier-Stokes equations defined in the domain $\Omega = \Omega_1 \cup \Omega_2 \cup \Gamma_f$, Ω_1 denotes fluid phase 1 and Ω_2 denotes fluid phase 2 and $\Gamma_f = \partial\Omega_1 \cap \partial\Omega_2$ is the interface between two fluid phases:

$$\rho_i \frac{D\vec{u_i}}{Dt} = -\nabla p_i + \nabla \cdot (\mu_i S_i) + \rho_i \vec{g} \qquad \in \Omega_i \tag{2.16}$$

$$\nabla \cdot \vec{u_i} = 0 \qquad \in \Omega_i \tag{2.17}$$

$$\vec{u_i}|_\Gamma = 0 \qquad \in \Omega_i \tag{2.18}$$

$$\vec{u_i}|_{t=0} = u_{0_i} \qquad \in \Omega_i \tag{2.19}$$

Where $i \in 1, 2$ and material derivative, $\frac{D\vec{u}}{Dt}$, is equal to $\frac{D\vec{u}}{Dt} = \frac{\partial\vec{u}}{\partial t} + \vec{u}.\nabla\vec{u}$. The viscous stress tensor is given by: $S_i := \nabla\vec{u_i} + \{\nabla\vec{u_i}\}^T$.The surface tension boundary condition at the interface is given by:

$$(T_1 - T_2).\vec{n} = \sigma\kappa\vec{n} \tag{2.20}$$

Where $T_i = -p_i + \mu_i S_i$ denotes the stress tensor, σ is the surface tension coefficient, κ is the local curvature, and $\vec{n}$ denotes the surface normal on Γ_f [38]. Furthermore, the velocity must be continuous across the free surface, i.e., $\vec{u_1} = \vec{u_2}$ on Γ_f.

2.2.1. Surface Tension Force Term

In order to couple the N-S Equation 2.16 with surface tension boundary condition, Equation 2.20, integral form of Equation 2.16 is written as:

$$\int_{\Omega_i} \rho_i \frac{D\vec{u_i}}{Dt}\, d\vec{x} = \int_{\partial\Omega_i} T_i.\vec{n}\, dF + \int_{\Omega_i} \rho_i.\vec{g}\, d\vec{x} \tag{2.21}$$

$$\rho_1 \int_{\Omega_1} \frac{D\vec{u}}{Dt}\, d\vec{x} + \rho_2 \int_{\Omega_2} \frac{D\vec{u}}{Dt}\, d\vec{x} = \int_{\partial\Omega} T.\vec{n}\, dF - \int_{\Gamma_f} [T].\vec{n}\, dF + \rho_1 \int_{\Omega_1} \vec{g}\, d\vec{x} + \rho_2 \int_{\Omega_2} \vec{g}\, d\vec{x} \tag{2.22}$$

where $T := T_1|_{\Omega_1} + T_2|_{\Omega_2}$ and [T] denotes the jump in the stress tensor T, i.e., $[T] = T_1 - T_2$, at the interface Γ_f. Applying the Gause theorem,

$$\int_{\partial\Omega} T.\vec{n}\, dF = \int_{\Omega} \nabla \cdot T\, d\vec{x} \tag{2.23}$$

Since the velocity is continuous across the interface, Equation 2.22 can be written as

$$\rho_1 \int_{\Omega_1} \frac{D\vec{u}}{Dt}\, d\vec{x} + \rho_2 \int_{\Omega_2} \frac{D\vec{u}}{Dt}\, d\vec{x} = \int_{\Omega} \rho \frac{D\vec{u}}{Dt}\, d\vec{x} \tag{2.24}$$

Now, by substituting (2.24) and (2.23) into (2.22), integral formulation of incompressible two-phase flow with surface tension is obtained as

$$\int_{\Omega} \rho \frac{D\vec{u}}{Dt}\, d\vec{x} = \int_{\Omega} \nabla \cdot T\, d\vec{x} - \int_{\Gamma_f} \sigma\kappa\vec{n}\, dF + \int_{\Omega} \rho\vec{g}\, d\vec{x} \tag{2.25}$$

In this way, surface tension boundary condition has been contained in the momentum equation as a free boundary integral. It is required to convert $\int_{\Gamma_f} \sigma\kappa\vec{n}\, dF$ term into a volume integral, so, it can be possible to couple the momentum equation with Level Set formulations and avoid explicit reconstruction of the interface. To this end, Continuum Surface Force (CSF) approach has been applied.

2.2.2. Continuum Surface Force approach

In (2.25) surface tension is included in the right-hand side as the source term. Since discretizations are based on differential expression of the Navier-Stokes equations, this free boundary integral needs to be converted to a volume integral. So, it is possible to obtain associated differential expression of the Navier-Stokes equation. To this end, a Level Set function, $\phi(\vec{x}, t)$ is applied to define the interface [25], i.e,

$$\Gamma_f(t) = \{\vec{x} \,:\, \phi(\vec{x}, t) = 0\} \tag{2.26}$$

using (2.26), the density, ρ,and viscosity, μ, can be easily defined on the whole domain through this Level Set function ϕ:

$$\rho(\phi) := \rho_2 + (\rho_1 - \rho_2)H(\phi) \qquad \text{and} \qquad \mu(\phi) := \mu_2 + (\mu_1 - \mu_2)H(\phi)$$

where $H(\phi)$ denotes the Heaviside function defined as

$$H(\phi) = \begin{cases} 0 & \text{if} \quad \phi < 0 \\ \frac{1}{2} & \text{if} \quad \phi = 0 \\ 1 & \text{if} \quad \phi > 0 \end{cases}$$

Now, Equation 2.25 can be written as a ϕ-dependent formulation

$$\int_\Omega \rho(\phi)\frac{D\vec{u}}{Dt}\, d\vec{x} = \int_\Omega \nabla \cdot T\, d\vec{x} - \int_{\Gamma_f} \sigma\kappa\vec{n}\, dF + \int_\Omega \rho(\phi)\vec{g}\, d\vec{x} \tag{2.27}$$

Due to Chang et al. [35] in the context of Level Set method, the free boundary integral can be converted into a volume integral using a Dirac δ-functional.

$$\int_{\Gamma_f} \sigma\kappa\vec{n}\, dF \;=\; \int_{\Omega} \sigma\kappa(\phi(\vec{x}))\delta(\phi(\vec{x}))\nabla\phi(\vec{x})\, d\vec{x} \tag{2.28}$$

Substituting (2.28) in (2.27) results in:

$$\int_{\Omega} \left(\rho(\phi)\frac{D\vec{u}}{Dt} \;-\; \nabla\cdot T \;+\; \sigma\kappa(\phi)\delta(\phi)\nabla\phi \;-\; \rho(\phi)\vec{g} \right) d\vec{x}$$

Therefore, the associated differential equation is

$$\rho(\phi)\frac{D\vec{u}}{Dt} \;-\; \nabla\cdot T \;+\; \sigma\kappa(\phi)\delta(\phi)\nabla\phi \;-\; \rho(\phi)\vec{g} \;=\; 0$$

With the definition of the stress tensor T, this yields to:

$$\rho(\phi)\frac{D\vec{u}}{Dt} \;+\; \nabla p \;=\; \nabla\cdot(\mu(\phi)S) \;-\; \sigma\kappa(\phi)\delta(\phi)\nabla\phi \;+\; \rho(\phi)\vec{g} \tag{2.29}$$

2.2.3. Smoothing

There is a sharp change in fluid properties across the interface which may lead to numerical instabilities. To avoid this, it is strongly suggested to consider an interface of thickness 2ε in which fluid properties such as density and viscosity change continuously as depicted in Figure 2.3. It is suggested to take ε approximately as $\varepsilon = 1.5dx$. Now,

$$\rho^{\varepsilon}(\phi) \;=\; \rho_2 \;+\; (\rho_1 \;-\; \rho_2)H^{\varepsilon}(\phi) \qquad \text{and} \qquad \mu^{\varepsilon}(\phi) \;=\; \mu_2 \;+\; (\mu_1 \;-\; \mu_2)H^{\varepsilon}(\phi) \tag{2.30}$$

Where H^{ε} denotes smoothed Heaviside function [33].

$$H^{\varepsilon}(\phi) = \begin{cases} 0 & \text{if} \quad \phi < -\varepsilon \\ \frac{1}{2}(1 + \frac{\phi}{\varepsilon} + \frac{1}{\pi}\sin(\frac{\pi\phi}{\varepsilon})) & \text{if} \quad |\phi| \leq \varepsilon \\ 1 & \text{if} \quad \phi > \varepsilon \end{cases} \tag{2.31}$$

The associated smoothed delta functional is given by :

$$\delta^{\varepsilon}(\phi) := \partial_{\phi} H^{\varepsilon} = \begin{cases} \frac{1}{2\varepsilon}\left(1 + \cos(\frac{\pi\phi}{\varepsilon})\right) & \text{for} \qquad |\phi| < \varepsilon \\ 0 & \text{elsewhere} \end{cases} \tag{2.32}$$

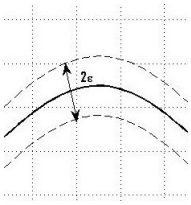


Figure 2.3. Thick Interface region.

2.2.4. Projection method

Instead of solving Navier-Stokes momentum equation in order to find $u^{\vec{n+1}}$ directly from $\vec{u^n}$, two-step approach is employed. Due to Chorin [39], first, intermediate velocity field $(\vec{u^{\star}})$ is computed via an explicit transport, neglecting pressure term. Then, a correction ∇p^{n+1} of the intermediate velocity field is done via the pressure Poisson equation which leads to a divergence free velocity field $u^{\vec{n+1}}$.

$$\frac{\vec{u^{\star}} - \vec{u^n}}{\delta t} = -(\vec{u^n}.\nabla)\vec{u^n} + \vec{g} + \ (\nabla \cdot (\mu(\phi^n)S^n) - \sigma\kappa(\phi^n)\delta(\phi^n)\nabla\phi^n) \tag{2.33}$$

$$\frac{\vec{u^{n+1}} - \vec{u^{\star}}}{\delta t} + \frac{\nabla p^{n+1}}{\rho(\phi^{n+1})} = 0 \tag{2.34}$$

$$\nabla \cdot \vec{u}^{n+1} = 0 \tag{2.35}$$

Applying divergence operator to (2.34) and subtract it from (2.35), the pressure Poisson equation is achieved

$$-\nabla \cdot \left(\frac{1}{\rho(\phi^{n+1})} \nabla \hat{p}^{n+1} \right) = -\nabla \cdot \vec{u}^{\star} \tag{2.36}$$

with $\hat{p}^{n+1} := \delta t p^{n+1}$.Biconjugate gradient method [40] with ILU pre conditioner is applied to solve Equation 2.36.

2.2.5. Discretization

Dicretizations are made in a staggered grid (like the sample shown in Figure 2.4) where several types of nodal points (velocity components, pressure, temperature, fluid properties (density and viscosity), vorticity, etc.), located in different geometrical positons, for example, scalar values like pressure (p) and Level Set function (ϕ) are located in the cell centers, while, vector values ($\vec{u}$ and $\vec{v}$) are located in faces (walls) of computational cells, as seen in Figure 2.5. While staggered grid allows for very natural and accurate formulation of several crucial partial differential equations (such as Stokes and Continuity equations) with finite differences and provide most simple and natural geometry of grid stencils needed for different equations, non-staggered rectangular grids (where all variables are defined in the same nodal points) may cause big problems in formulating equations with finite differences because variables are not located in optimal positions [42]. That is why we prefer staggered grid in this study.

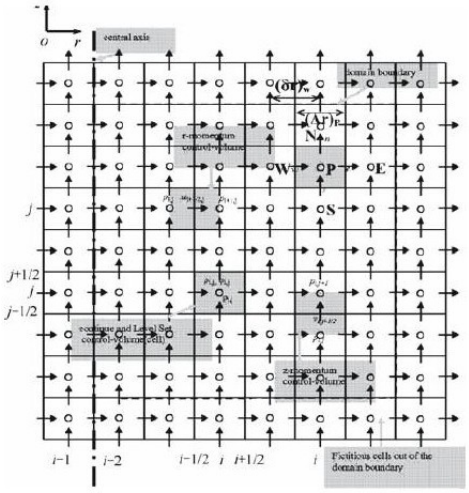


Figure 2.4. Staggered grid.

[41]

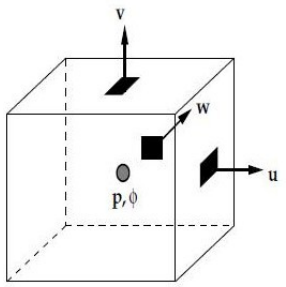


Figure 2.5. Position of variables in computational cell.

[38]

2.2.6. Derivation

The computation of the intermediate velocity, $\vec{u}^{\star}$, requires the discretization of the viscous terms, $\nabla \cdot (\mu(\phi^n)S^n)$, in the nodes where velocity is defined. Hence, the x and y-component of the viscous term is

$$2\left(\mu(\phi)u_x\right)_x + \left(\mu(\phi)(u_y + v_x)\right)_y \tag{2.37}$$

$$\left(\mu(\phi)(u_y + v_x)\right)_x + 2\left(\mu(\phi)v_y\right)_y \tag{2.38}$$

The first derivative of the velocities can be computed with central differences as follows

$$[u_x]_{i,j} \;=\; (dx)^{-1}(u_{i+\frac{1}{2},j} \;-\; u_{i-\frac{1}{2},j})$$

$$[u_y]_{i+\frac{1}{2},j+\frac{1}{2}} \;=\; (dy)^{-1}(u_{i+\frac{1}{2},j+1} \;-\; u_{i+\frac{1}{2},j})$$

For second order derivatives, the terms in (2.37) are approximated, for example, at u positions $(i+\frac{1}{2}, j+\frac{1}{2})$

$$[2\left(\mu(\phi)u_x\right)_x] \;=\; 2(dx)^{-1}\left(\mu(\phi_{i+1,j})[u_x]_{i+1,j} \;-\; \mu(\phi_{i,j})[u_x]_{i,j}\right)$$

$$\begin{aligned}[(\mu(\phi)(u_y \;+\; v_x))_y]_{i+\frac{1}{2},j} = \;& (dy)^{-1} \;\left(\mu(\phi_{i+\frac{1}{2},j+\frac{1}{2}})[u_y + v_x]_{i+\frac{1}{2},j+\frac{1}{2}}\right) \;- \\ & (dy)^{-1} \;\left(\mu(\phi_{i+\frac{1}{2},j-\frac{1}{2}})[u_y + v_x]_{i+\frac{1}{2},j-\frac{1}{2}}\right)\end{aligned}$$

2.2.7. Interpolation

Obviously from above equations, for required derivations we need to find values of some variables in nodal points in which the other variable is located. For example, in Equation 2.37, in order to calculate the second term, we should have the values of fluid viscosity at $i+\frac{1}{2}, j+\frac{1}{2}$, cell corners, while, the actual values are preserved in cell centers. To achieve this aim, interpolations are required. In this study, third order lagrange interpolation scheme is applied. For example, the approximation of u in x-direction is calculated as follows

$$\text{centered }: u_{i,j} \;=\; \frac{1}{16}\left(-u_{i-\frac{3}{2},j} \;+\; 9u_{i-\frac{1}{2},j} \;+\; 9u_{i+\frac{1}{2},j} \;-\; u_{i+\frac{3}{2},j}\right)$$

$$\text{left-weighted } :u_{i,j} \;=\; \frac{1}{16}\left(5u_{i-\frac{1}{2},j} \;+\; 15u_{i+\frac{1}{2},j} \;-\; 5u_{i+\frac{3}{2},j} \;+\; u_{i+\frac{5}{2},j}\right)$$

$$\text{right-weighted } :u_{i,j} \;=\; \frac{1}{16}\left(u_{i-\frac{5}{2},j} \;-\; 5u_{i-\frac{3}{2},j} \;+\; 15u_{i-\frac{1}{2},j} \;+\; 5u_{i+\frac{1}{2},j}\right)$$

Also, some velocity values need to be interpolated to cell face centers. For example, the velocity value v at nodes occupied by u values $(i+\frac{1}{2}, j)$ is given by

$$\begin{aligned} v_{i+\frac{1}{2},j} \;=\; \frac{1}{32}(\quad & -v_{i-1,j+\frac{3}{2}} - v_{i-1,j-\frac{3}{2}} - v_{i+2,j+\frac{3}{2}} - v_{i+2,j-\frac{3}{2}} + \\ & 9v_{i,j+\frac{1}{2}} + 9v_{i,j-\frac{1}{2}} + 9v_{i+1,j+\frac{1}{2}} + 9v_{i+1,j-\frac{1}{2}}) \end{aligned}$$

in Figure 2.6, the above equations were depicted.

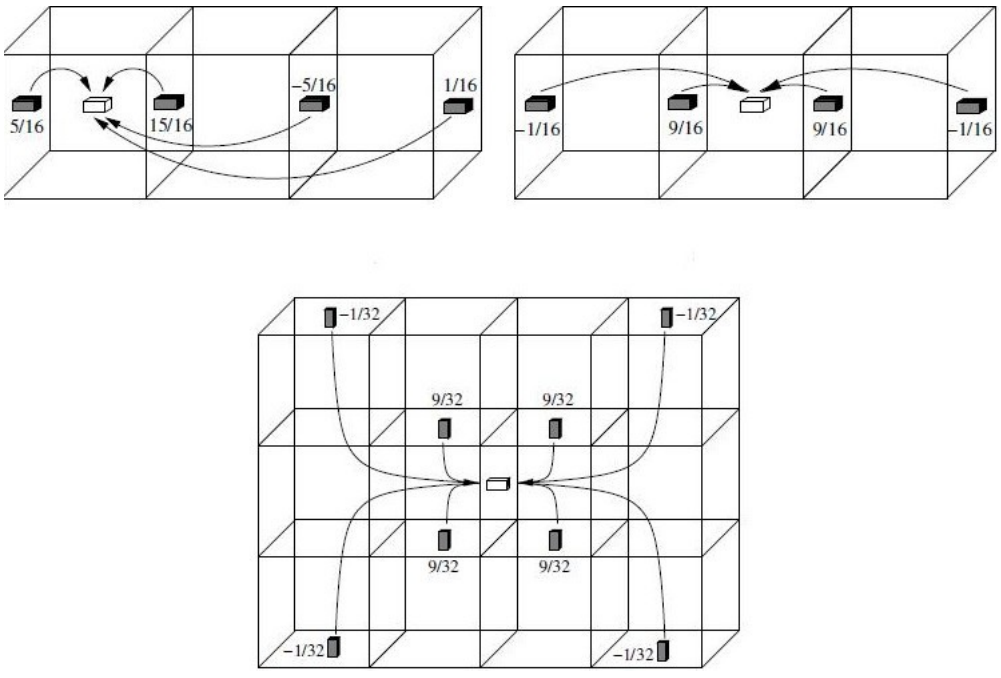


Figure 2.6. Third order lagrange interpolation scheme.

[38]

2.3. Non-dimensionalization

It is better to change Equation 2.29 into non-dimensional form in order to analyze the effects of some non-dimensional parameters in the flow such as Reynolds and Eotvos numbers which are defined as $Re = \frac{\rho_1 V L}{\mu_1}$ and $Eo = \frac{\rho_1 V^2 L}{\sigma}$. Where L is a characteristic length, V is a characteristic velocity which is equal to $V = \sqrt{gL}$, and σ is surface tension coefficient. $\bar{\rho}$ and $\bar{\mu}$, non-dimensional density and viscosity, are defined as $\bar{\rho} = \frac{\rho}{\rho_1}$ and $\bar{\mu} = \frac{\mu}{\mu_1}$, where ρ_1 and μ_1 are base density and viscosity. Using these non-dimensional terms, Equation 2.29 is changed to

$$\frac{\partial \vec{u}}{\partial t} = -\vec{u} \cdot (\nabla \vec{u}) - \frac{1}{\bar{\rho}(\phi)} \{\nabla p + \frac{1}{Re}(\nabla \cdot (\bar{\mu}(\phi) S)) - \frac{1}{Eo}(\kappa \delta \nabla \phi) + \vec{e}\} \tag{2.39}$$

where $S = \nabla \vec{u} + \{\nabla \vec{u}\}^T$ and $\vec{e}$ is a unit vector.

2.4. Mass Conservation

In order to show the conservation of mass or volume, fraction of mass at a time step to the mass of initial state is calculated as follows,

$$Mass fraction = \frac{\Sigma_{i,j} \rho_{i,j}(\vec{x}, t = 0) dx dy}{\Sigma_{i,j} \rho_{i,j}(\vec{x}, t) dx dy} \tag{2.40}$$

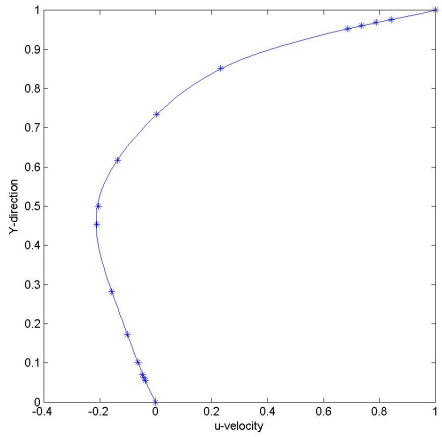
This mass fraction is desired to be 1.

3. Results and Discussion

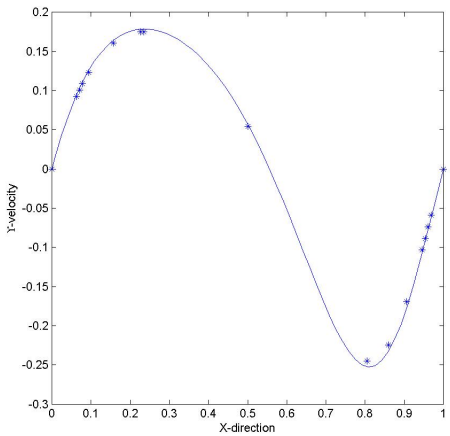
In order to test and validate the projection method applied in the solution of Navier-Stokes equation procedure, Lid Driven Cavity test case for one-phase flow is considered. Moreover, the ability of Level Set method in handling two-phase flows is tested via four test case problems, Rayleigh-Taylor Instability, Rising Bubble, Droplet Fall, Bursting Bubble at the Free Surface, and Droplet Fall onto the Free Surface. Comparisons are done with results obtained by Ghia [43] for Lid Driven Cavity problem. For two-phase test case problems, comparison is done with results obtained by SPH method.

3.1. Code Validation

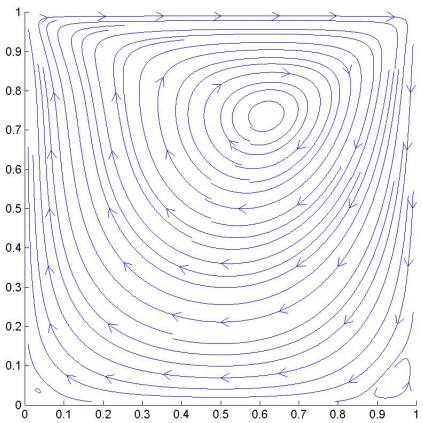
To be sure of correctness of projection method applied in momentum equation, a one-phase test case study of Lid Driven cavity is considered. Imagine a square domain of non-dimensional length of 1 which is filled with an incompressible fluid and the top wall or the Lid is driven with a constant non-dimensional velocity of 1. No-slip boundary condition is applied to all walls except the Lid. The grid numbers used for this test case is 60×60. Results are compared with the work of Ghia [43] for three Reynolds numbers, $Re = 100$, $Re = 400$, and $Re = 1000$.Changes of velocity in x and y directions from bottom to top and left to right in the middle of the cavity for $Re = 100$, $Re = 400$, and $Re = 1000$ are depicted in figures (3.1) to (3.3). Results obtained by Ghia are assigned with $*$ sign. Good agreement between two methods is observed.



u-velocity

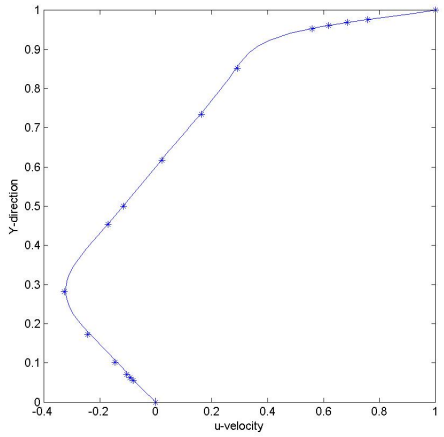


v-velocity

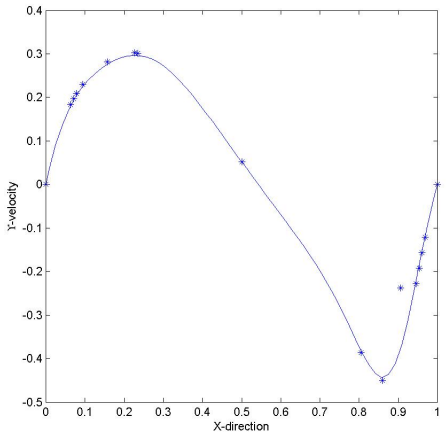


Streamline

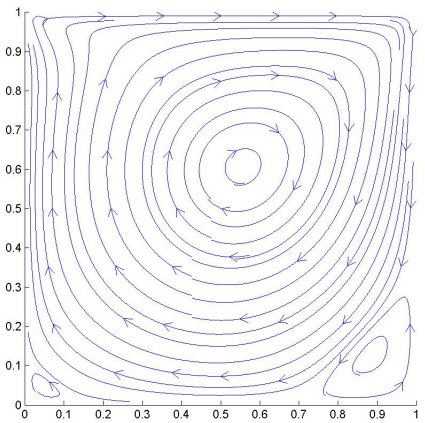
Figure 3.1. u and v velocity components and streamline for $Re = 100$.



u-velocity

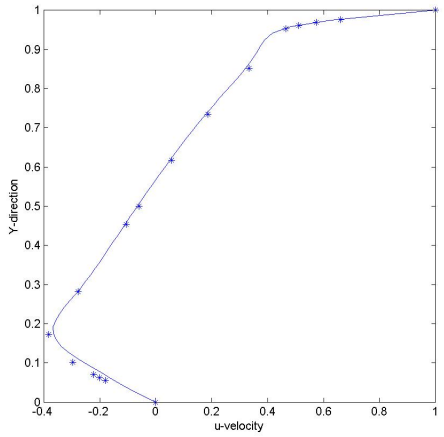


v-velocity

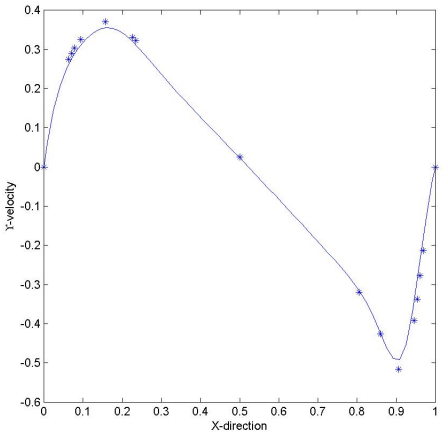


Streamline

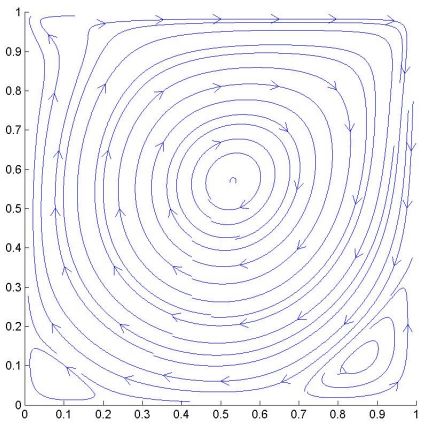
Figure 3.2. u and v velocity components and streamline for $Re = 400$.



u-velocity



v-velocity



Streamline

Figure 3.3. u and v velocity components and streamline for $Re = 1000$.

In this study, LS method is compared with ISPH method for two-phase incompressible immiscible fluid flows via five test cases: Rayleigh Taylor instability, Rising Bubble, Droplet Fall, Bursting Bubble and Droplet Fall onto a Free Surface. We examine the behavior of these methods for handling difficulties arising in these test cases such as high Reynolds number, high density and viscosity ratio, splashing of a droplet on a solid surface and topological changes like merging and pinching off.

In order to make a better comparison of these methods, we make certain adjustments. Firstly, we set half of the interface thickness in LS as $\varepsilon = 4dx$. This is approximately equal to radius of neighborhood of a particle in SPH, $3h \approx 4dx$. Therefore, density and viscosity are smoothed in a region across the interface that has approximately same thickness in both methods. Another adjustment is that we do not consider surface tension in our calculations. This is because surface tension models possess differences in LS and SPH.

For LS simulations, 60×60 grids are used while for SPH simulation, 3600 particles are used. The geometry is a square cavity of dimensionless length 1 for all test cases. Reynolds number is defined as $Re = \frac{\rho_1 V L}{\mu_1}$ where characteristic velocity, V, is defined as $V = \sqrt{gL}$, ρ_1 and μ_1 correspond to density and viscosity of heavier fluid respectively. Results are depicted in dimensionless time step for each test case where $\bar{t} = \sqrt{L/g}$ is the characteristic time scale.

3.2. Rayleigh-Taylor Instability

In this first test case, Rayleigh-Taylor Instability problem is considered in order to show the ability of LS and SPH methods in capturing evolution of interface. In this phenomenon, a heavier fluid is accelerated into a lighter one due to gravity with an initial perturbation at the interface between two fluids. We considered a square domain filled by two fluids with different densities while the heavier one placed on the top of the lighter one.

Density and viscosity ratios are chosen to be $\rho_1/\rho_2 = 2$ and $\mu_1/\mu_2 = 1$ respectively, and the Reynolds number is set to be $Re = 400$. The initial perturbation is imposed by defining the sinusoidal function like $Y = Asin(\omega x) - Y_0$ at the interface where A is the amplitude and ω is the frequency of this perturbation. We took $A = 0.15$, $\omega = 2\pi$, and $Y_0 = 0.5$. As depicted in Fig(3.4), great agreement between LS and SPH simulation of interface evolution at different times is achieved.

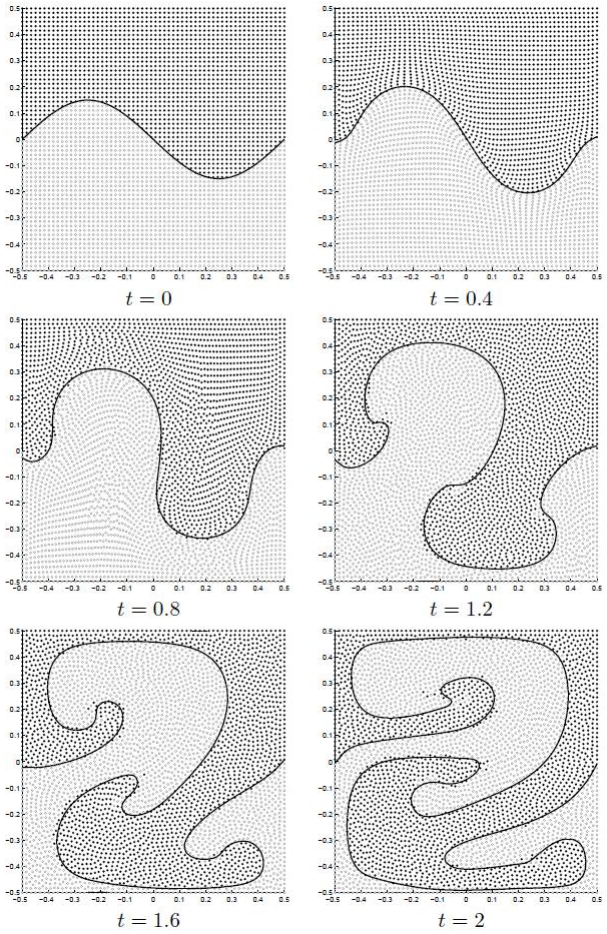


Figure 3.4. Rayleigh-Taylor Instability: — represent Level Set Function, ● represents high density particles and ○ represents low density particles.

According to Chandrasekhar [44], there is a critical value for surface tension coefficient in which the flow is stabilized. This critical value is given by

$$\sigma_c = \frac{\lambda^2(\rho_1 - \rho_2)g}{4\pi^2} \tag{3.1}$$

where λ is a wavelength of initial perturbation. In order to show the effect of surface tension on the evolution of the interface, two different cases, with and without surface tension, are considered.

Computational domain in this test case is a rectangle $(0; 1) \times (0; 4)$, densities of two fluids are $\rho_1 = 1.2kg/m^3$ and $\rho_2 = 0.17kg/m^3$, and viscosities of both fluids are $\mu_1 = \mu_2 = 0.003kg/(m \cdot s)$, the surface tension coefficient is zero, and computations are done in a rectangular domain, 40×160. The initial interface perturbation is given by $Y - 0.05\cos(2\pi x) - 2$. As heavier fluid penetrates the lighter one, the interface takes a mushroom shape. This phenomenon which is known as Kelvin-Helmholtz instability is depicted in Figure 3.5.

For previous test case, according to Equation 3.1, critical value of surface tension is $\sigma_c = 0.026$. Figure 3.6 shows the evolution for the problem same as previous one but in the presence of surface tension smaller than the critical value, $\sigma = 0.015$. It is seen that surface tension makes the penetration process slower, delays the Kelvin-Helmholtz instability formation, and reduces the interface deformations.

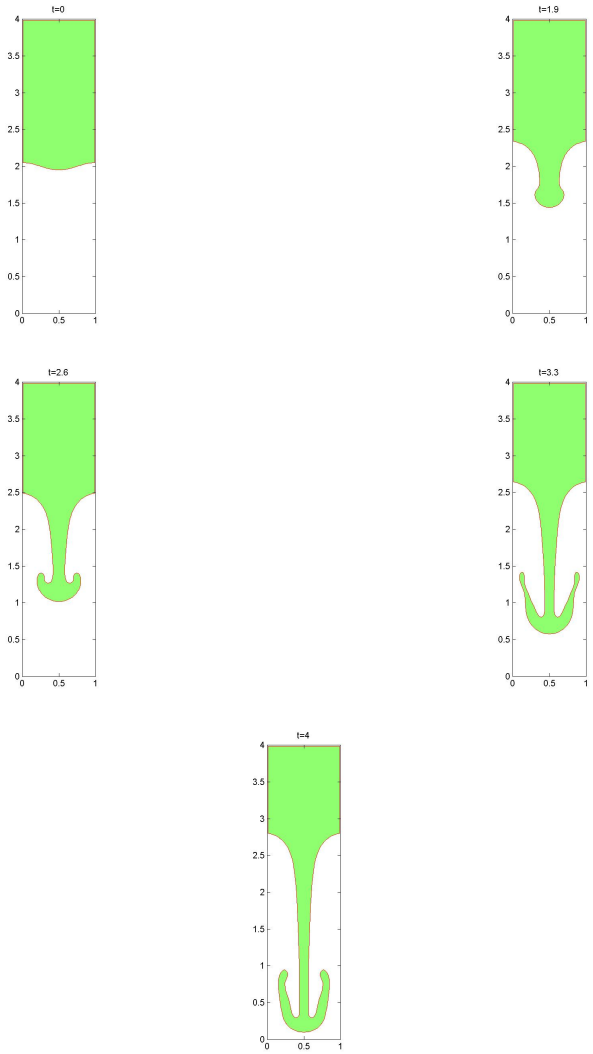


Figure 3.5. Rayleigh-Taylor Instability without surface tension.

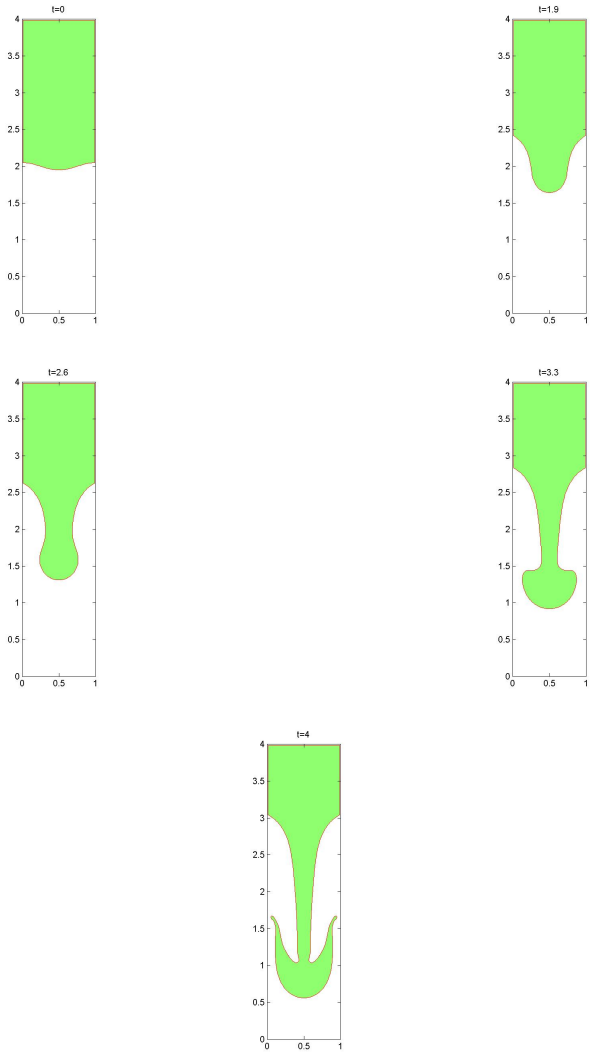


Figure 3.6. Rayleigh-Taylor Instability with small surface tension, $\sigma = 0.015$.

3.3. Rising Bubble

Another test case is rising gas bubble in a surrounding liquid. This is a well known and very important problem in multiphase flows for those dealing with bubbly flows. In this case, we take an extremely large density ratio, $\rho_1/\rho_2 = 1000$, a large viscosity ratio, $\mu_1/\mu_2 = 100$, and a high Reynolds number, $Re = 1000$. Initially, bubble has a radius of $R = 0.125$ and its center is located at $(x_c, y_c) = (0, -0.3)$. The Level Set function is defined as $\phi = \sqrt{(x - x_c)^2 + (y - y_c)^2} - R$. The lighter gas bubble experiences shape changes while it is rising due to buoyancy forces.

Although both methods show relatively good agreement at first time steps, as depicted in Figure 3.7, little differences appear later on. This may be due to lack of mass conservation or relatively large smoothing length, ε, in LS.

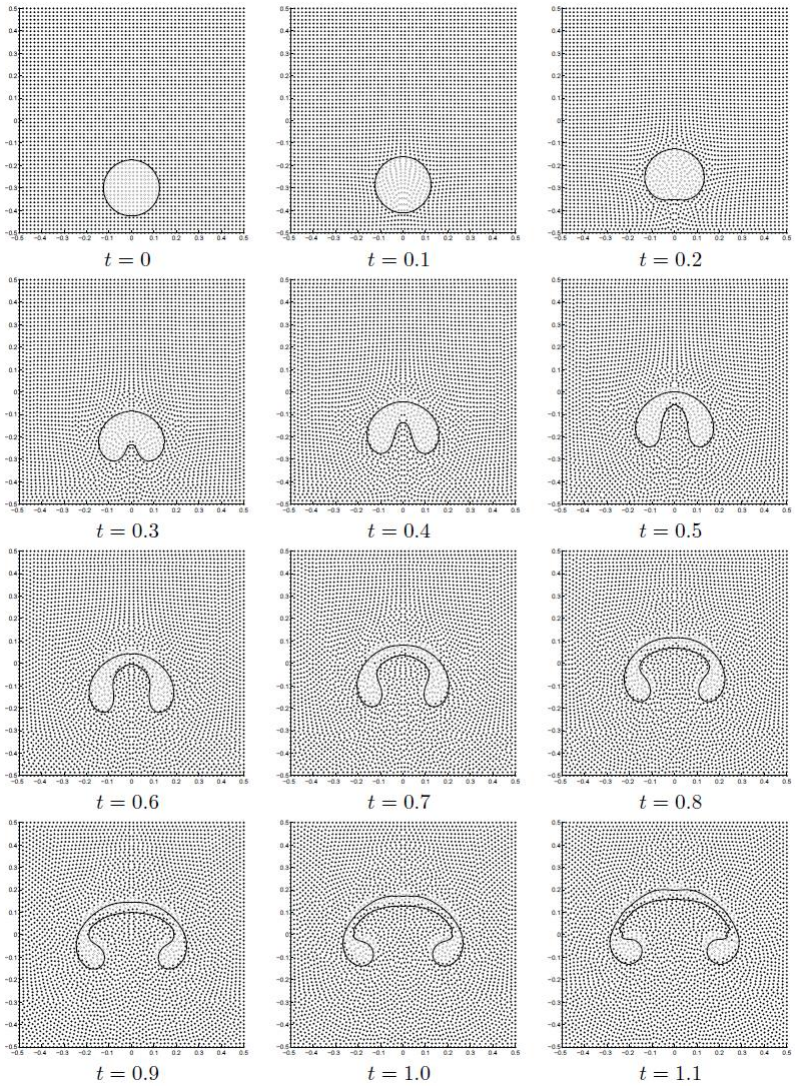
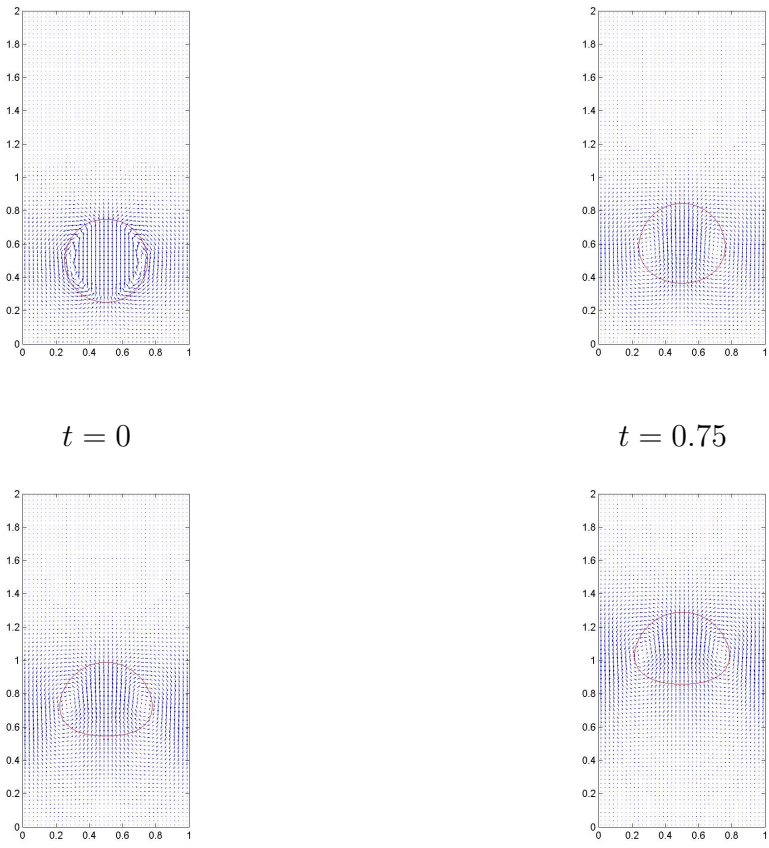


Figure 3.7. Rising Bubble: — represent Level Set Function, ● represents high density particles and ○ represents low density particles.

There are some non-dimensional parameters such as Reynolds number (Re), Eotvos number (Eo), density ratio, and viscosity ratio that affect the elevation of bubble among the surrounding fluid. Beyond the effects of these parameters, effect of grid resolution is also investigated. Moreover, effects of bubbles on each other, while they are rising in the surrounding fluid is investigated.

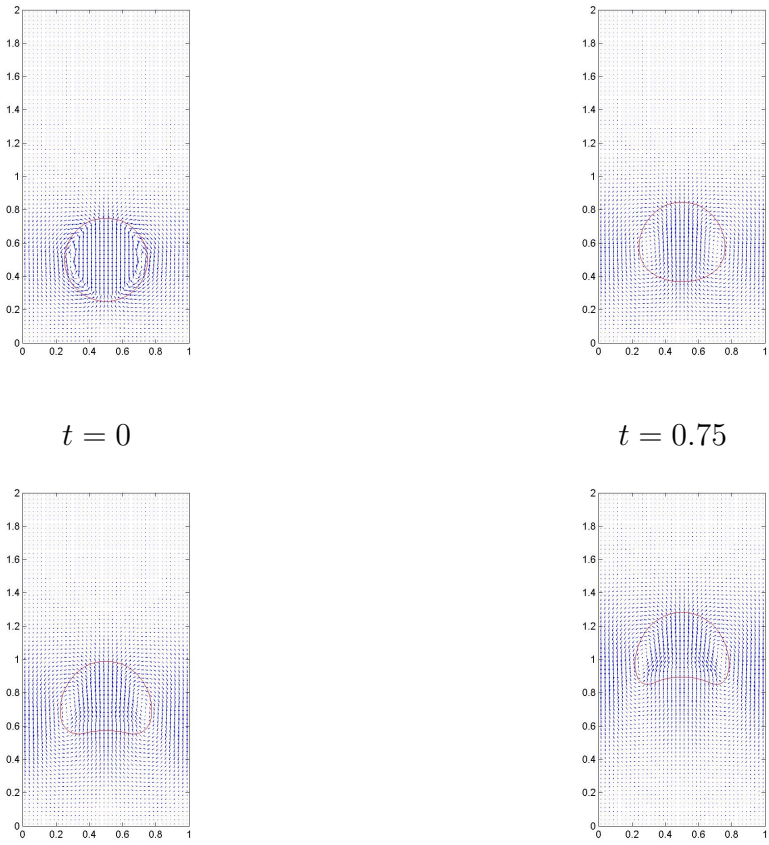
The computational domain for Rising Bubble test case is set to $(0;1) \times (0;2)$ and the initial shape of bubble is supposed to be a circle with center $(0.5, 0.5)$ and radius $R = 0.25$. Free-slip and no-slip boundary conditions are imposed to vertical and horizontal walls respectively. Density and viscosity ratios are $\rho_1/\rho_2 = 1000$ and $\mu_1/\mu_2 = 100$ respectively. Reynolds number is set to $Re = 35$, but in order to investigate the effect of surface tension, different Eotvos numbers, $Eo = 25$ and $Eo = 125$, are considered. The shape changes that bubble experiences during its elevation is depicted in Figures 3.8 and 3.9 for both cases. Computations are done in 40×80 rectangular grid. As it is obvious from Figures 3.8 and 3.9, shape changes in the case of high Eotvos number (low surface tension coefficient) is more tense than the case of low Eotvos number (high surface tension coefficient). It means that surface tension force term restricts deformation of bubble during its evolution.



$t = 0$ $t = 0.75$

$t = 1.5$ $t = 3$

Figure 3.8. Rising Bubble with low Eo number ($Eo = 25$ and $Re = 35$).

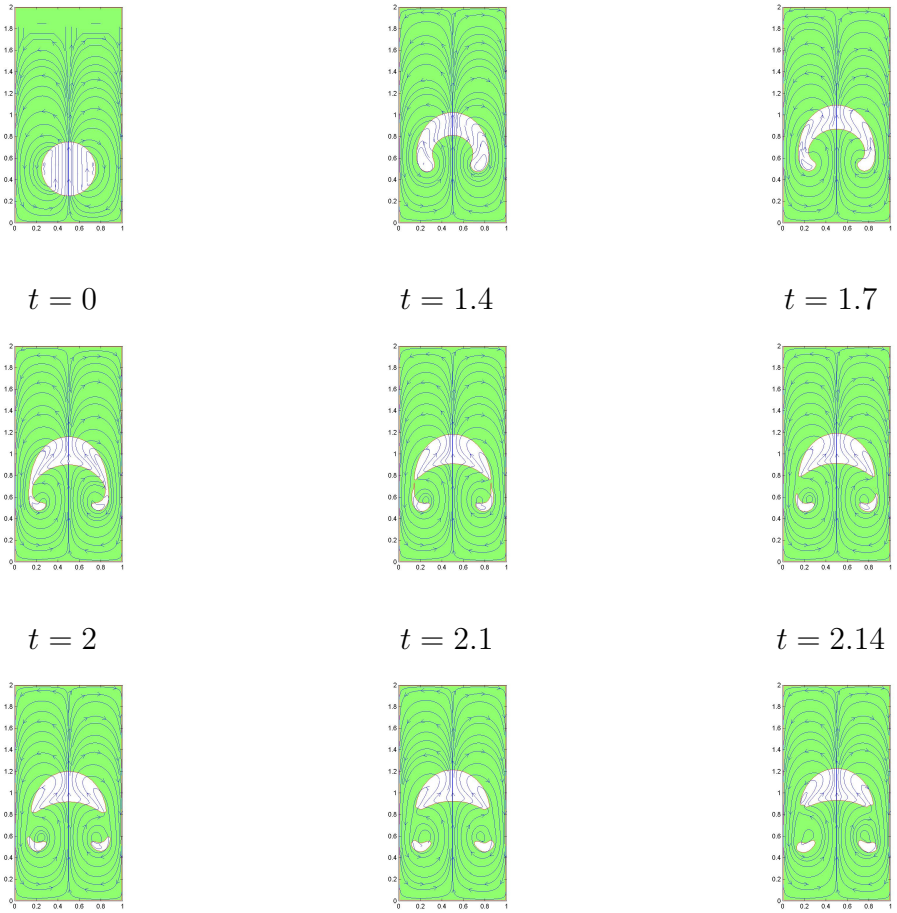


$t = 0$ $t = 0.75$

$t = 1.5$ $t = 3$

Figure 3.9. Rising Bubble with high Eo number ($Eo = 125$ and $Re = 35$).

In the next test case, Eotvos and Reynolds numbers are increased to $Re = 700$ and $Eo = 500$ and all other parameters are remained the same as previous test case. Since Eotvos number is relatively high, bubble will catch the skirted shape as time goes on. In high Reynolds numbers as in this test case, vortices that are created in the wake of bubble cause more intense circulations that leads to seperation of bubble skirts. Evolution and pinching off process are captured in Figure 3.10.



$t = 0$ $t = 1.4$ $t = 1.7$

$t = 2$ $t = 2.1$ $t = 2.14$

$t = 2.18$ $t = 2.24$ $t = 2.3$

Figure 3.10. Pinching off process in Rising Bubble, $Re = 700$ and $Eo = 500$. Computaions are based on 80×160 rectangle grid.

In order to show the effect of grid resolution, computations for previous test case is done in three different grids, 20×40, 40×80 and 80×160. Results are compared in Figure 3.13 for $t = 2.1$. Also, diagram of mass conservation for three grids is depicted in Figure 3.14.

Now, the effect of bubbles on each other during their elevation is considered. Here, two circular bubbles are centered at $(0.5, 1)$ and $(0.5, 0.5)$ with radii $R = 0.25$ and $R = 0.2$ respectively. Computational domain is set to $(0; 1) \times (0; 2)$ with a rectangular grid, 40×80. Reynolds number is $Re = 700$ and Eotvos number is $Eo = 500$. Two opposite vortices which are created in the wake of upper bubble, generates a low pressure field and make the lower bubble rise faster that leads to merging of two

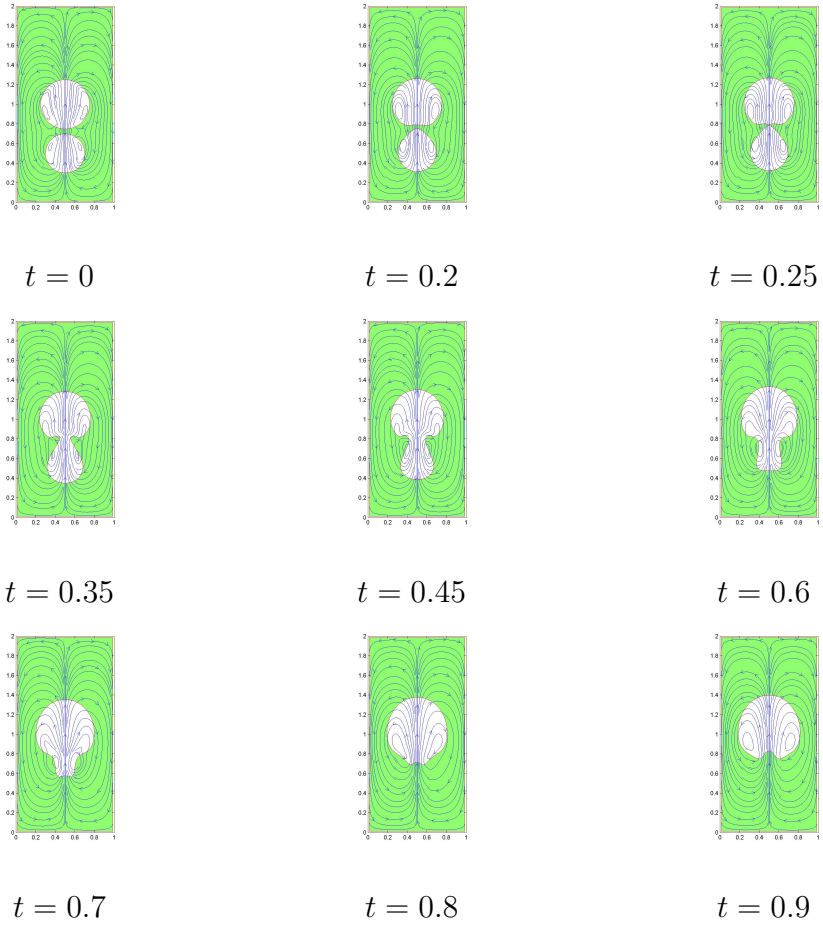
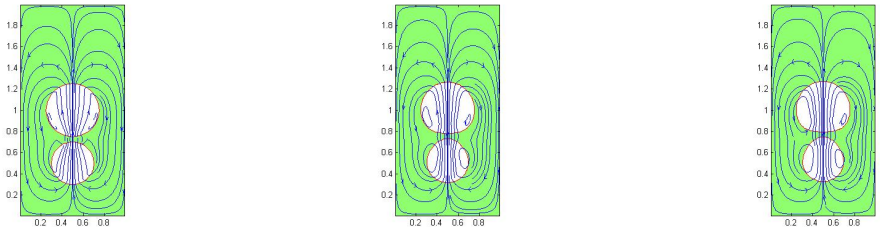
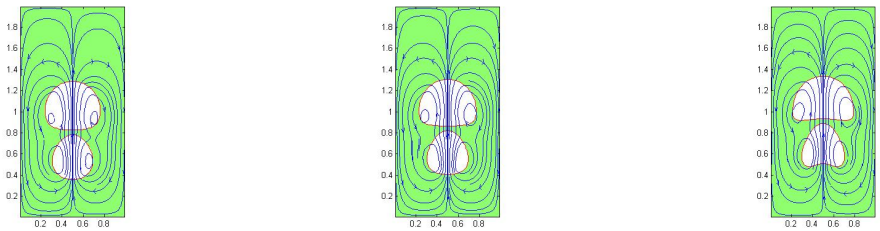


Figure 3.11. Merging of two bubbles, $Eo = 500$.

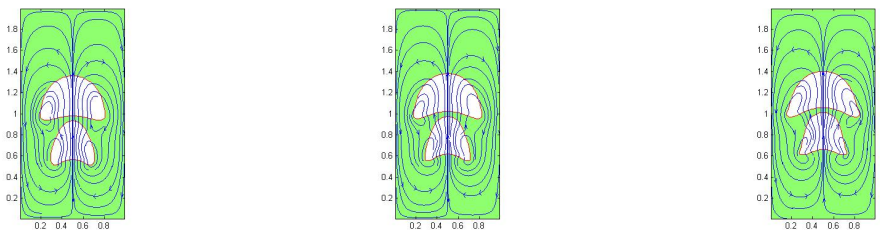
bubbles as depicted in Figure 3.11. Note that the merging process is closely rlated to the initial distance between two bubbles and the surface tension coefficient. If two bubbles are relatively far from each other and surface tension is high enough (small Eotvos number), merging of two bubbles will not happen. Figure 3.12 shows the evolution of rising two bubbles without merging together, where the Eotvos number is very low ($Eo = 50$) that means high surface tension coefficient and Reynolds number is remained as the same as previous test case, $Re = 700$.



$t = 0$ $t = 0.2$ $t = 0.25$

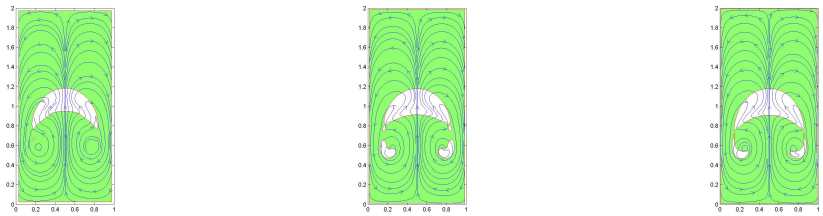


$t = 0.35$ $t = 0.45$ $t = 0.6$



$t = 0.7$ $t = 0.8$ $t = 0.9$

Figure 3.12. Rising of two bubbles without merging, $Eo = 50$.



(a) (b) (c)

Figure 3.13. Grid resolution, a) 20×40, b) 40×80, c) 80×160.

3.4. Droplet Fall

A similar but opposite case of rising bubble problem is the falling of denser fluid in the surrounding lighter fluid. Reynolds number, density and viscosity ratios are set as Rising Bubble test case which is compared with SPH method. Initially, bubble has a radius of $R = 0.125$ and its center is located at $(x_c, y_c) = (0, 0.3)$. The Level Set

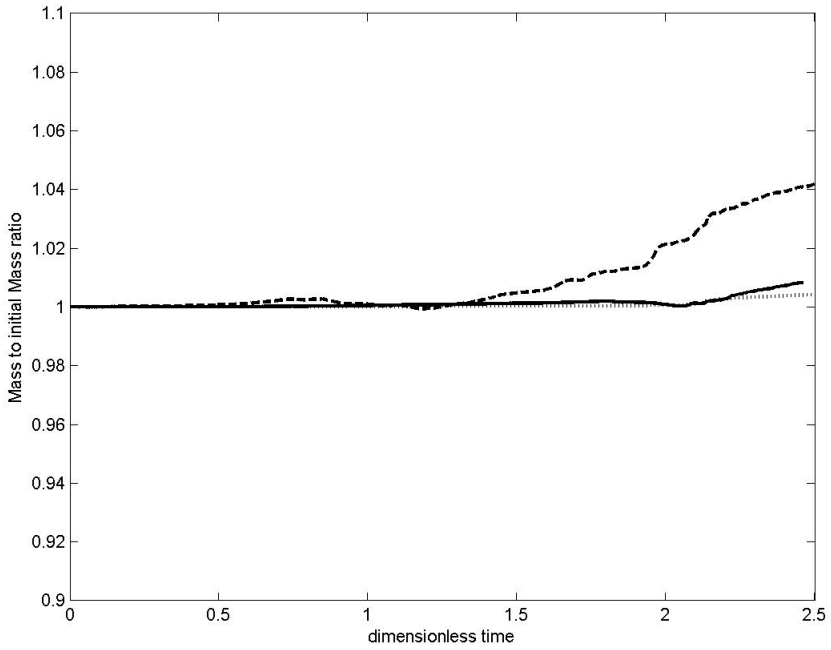


Figure 3.14. Mass conservation diagram for three different grids. "- -": 20×40, "-": 40×80, "$\cdots$": 80×160.

function is defined as $\phi = R - \sqrt{(x - x_c)^2 + (y - y_c)^2}$. It is observed that liquid droplet splashes as it hits the ground and spreads in two sides on the ground surface. Results obtained by two methods are depicted in Figure 3.15. Both methods showed satisfying performance in capturing the interface and its evolution during the whole simulation.

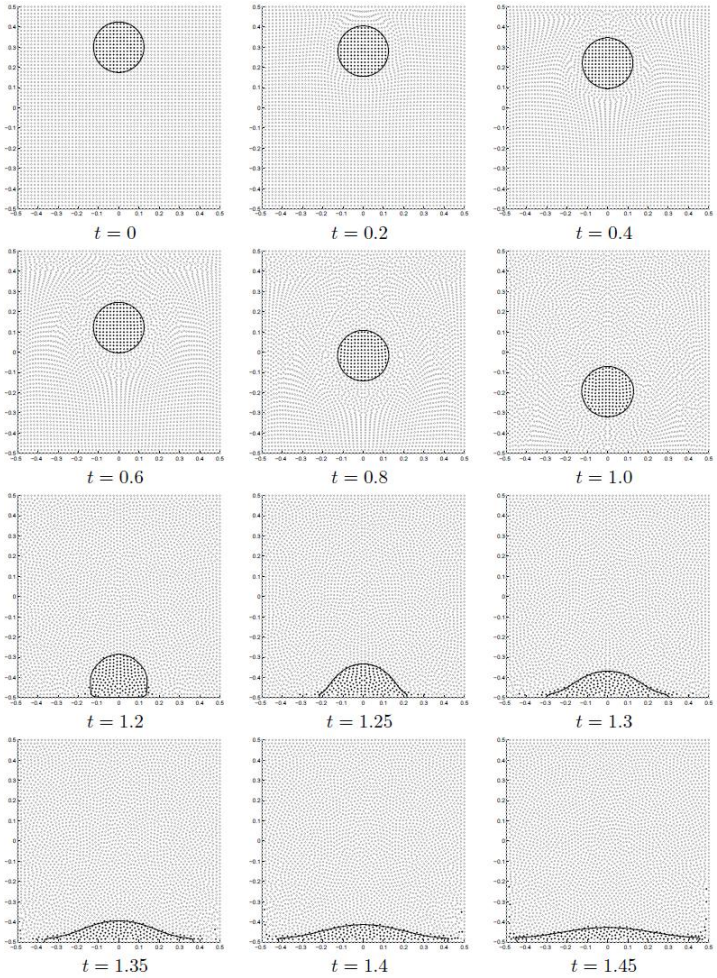


Figure 3.15. Droplet Fall: — represent Level Set Function, ● represents high density particles and ○ represents low density particles.

3.5. Bursting Bubble at the Free Surface

In this case, bubble rises until it meets and merges with the free surface. Similarly, Reynolds number, density and viscosity ratios are the same as previous cases ($Re = 1000, \frac{\rho_1}{\rho_2} = 1000, \frac{\mu_1}{\mu_2} = 100$). Initially, free surface is located at $y_s = -0.2$, bubble has a radius of $R = 0.125$ and its center is located at $(x_c, y_c) = (0, -0.35)$. The Level Set function is defined by defining two functions $\phi_1 = \sqrt{(x - x_c)^2 + (y - y_c)^2} - R$, $\phi_2 = y_s - y$ and taking the minimum of them $\phi = min(\phi_1, \phi_2)$. It is seen that a fluid jet is formed after bubble merges with the free surface.

Although both LS and SPH could capture merging and jet formation phenomena, we observe differences in LS and SPH results in terms of drop release. For instance, SPH captures fluid drops emanating from the liquid film above the bubble at the initial state and the fluid jet formed after the merging while we do not see these drops in LS results. It may be due to lack of mass conservation or large smoothing length in LS method.

As mentioed earlier, surface tension was neglected in order to make better comparison with SPH method. Here, bursting and jet formation phenomena are considered in the presence of surface tension with Eotvos number of $Eo = 300$, while the other parameters are kept the same. As it is obvious from Figure 3.17 the fluid jet, which is formed after merging of bubble with the free surface, is shorter in comparison with the case without surface tension force term.

Beyond surface tension or value of the Eotvos number, Initial distance between bubble and the free surface is also effective in formation of fluid jet. In Figure 3.18 free surface is initially located further from bubble and no fluid jet is formed after bubble merges with the free surface. When bubble is close enough to the free surface, high pressure difference that occurs at very small region leads to formation of fluid jet. On the other hand, in the case that bubble is far from the free surface, pressure difference is not that much high to produce a fluid jet. Figure 3.19 explains this situation.

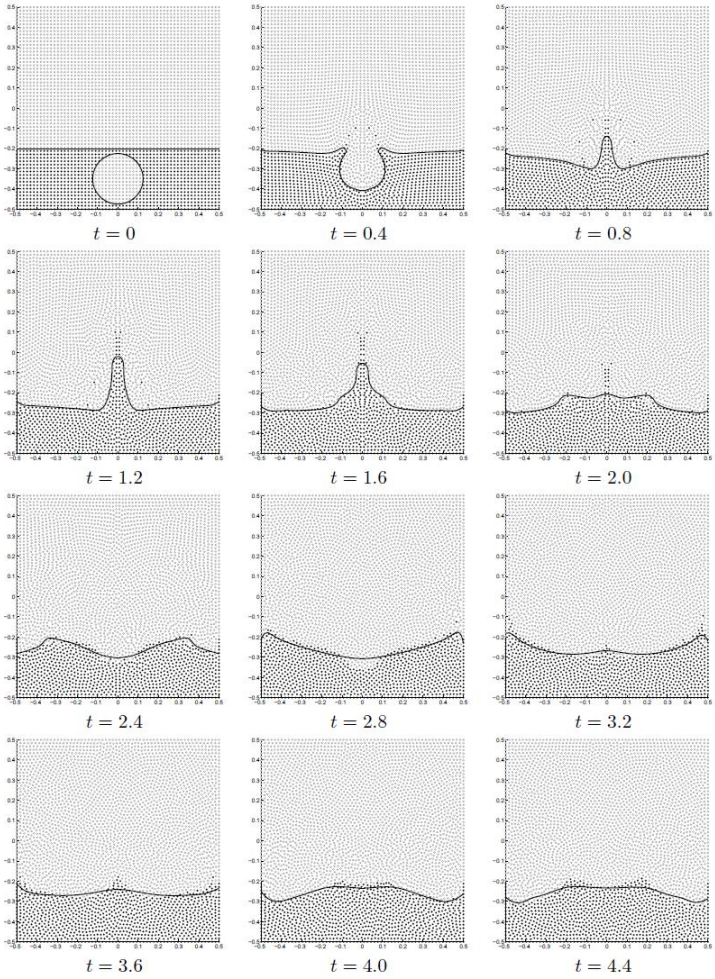
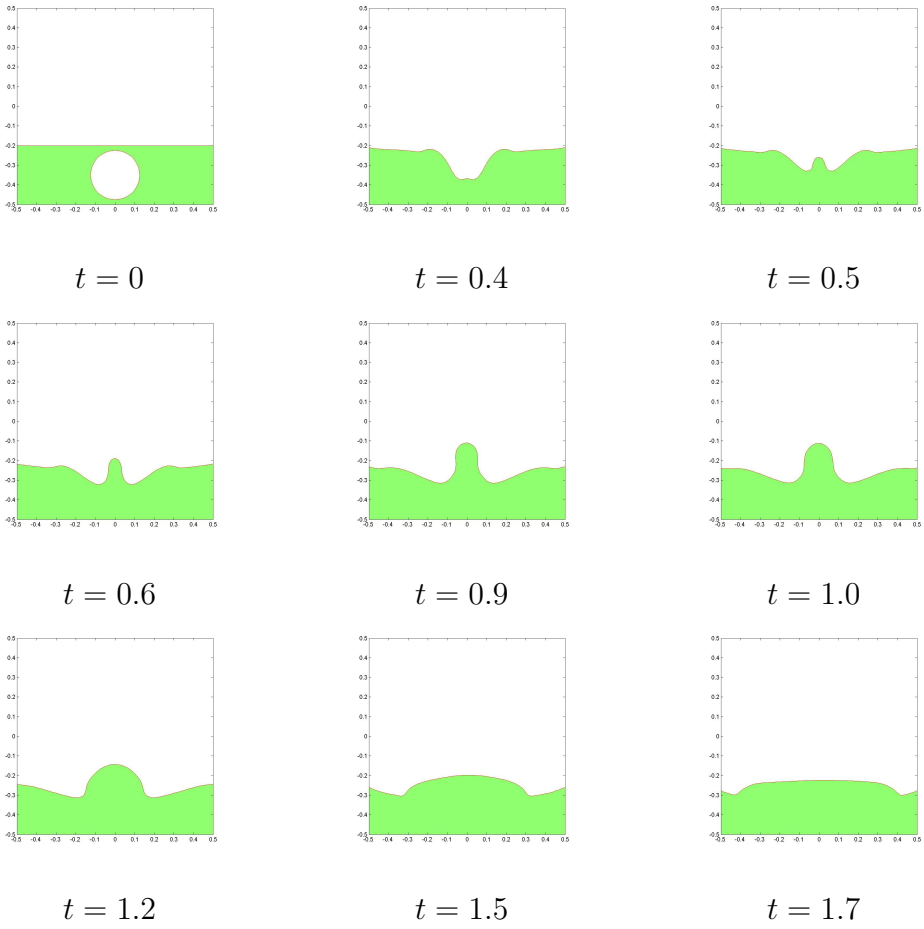


Figure 3.16. Bursting Bubble: — represent Level Set Function, ● represents high density particles and ○ represents low density particles.

3.6. Droplet Fall onto the Free Surface

In this test case, droplet falls into a free surface and merges with it. This is the opposite case of the bursting bubble problem. Reynolds number, density and viscosity ratios are the same as bursting bubble case. Initially, free surface is located at $y_s = -0.2$, bubble has a radius of $R = 0.125$ and its center is located at $(x_c, y_c) = (0, -0.05)$. The Level Set function is defined by defining two functions $\phi_1 = R - \sqrt{(x - x_c)^2 + (y - y_c)^2}$, $\phi_2 = y - y_s$ and taking the maximum of them $\phi = max(\phi_1, \phi_2)$. The results obtained by LS and SPH show good agreement in this case. However, SPH captures that gas bubbles just below the liquid droplet at the initial state are trapped and dispersed in liquid as droplet merges with free surface.



$t = 0$ $t = 0.4$ $t = 0.5$

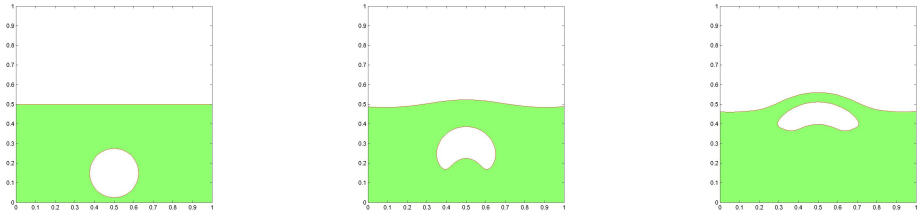
$t = 0.6$ $t = 0.9$ $t = 1.0$

$t = 1.2$ $t = 1.5$ $t = 1.7$

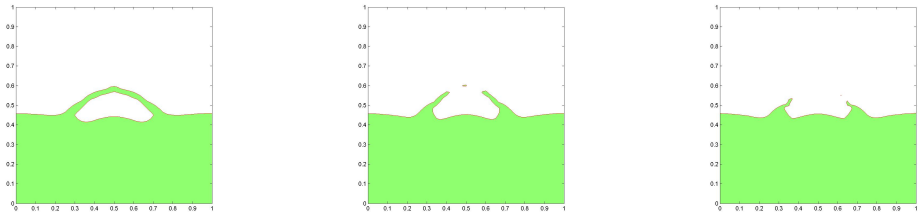
Figure 3.17. Bursting Bubble with jet formation in the presence of surface tension, $Eo = 300$.

3.7. Dam Breaking

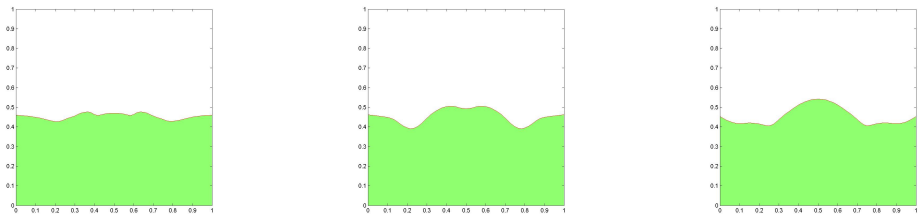
Here, collapsing of fluid column, which is also known as Dam Breaking problem, is considered. Computational domain is $(0; 3.22) \times (0; 2)$, fluid densities are $\rho_1 = 998.2kg/m^3$ and $\rho_2 = 1.225kg/m^3$, and viscosities are $\mu_1 = 0.01137kg/(m.s)$ and $\mu_2 = 1.78 \times 10^-4kg/(m.s)$, and surface tension force term is neglected. Figures 3.21 and 3.22 show the evolutions for two cases, without and with obstacle, respectively. The obstacle is placed in $X = 2.24$ with length of 0.16 and height of 0.21 to show the behaviour of the fluid when it hits the solid obstacle. Figure 3.23 shows the pressure field for Dam Breaking with obstacle case. As it is obvious from the figure, impact of fluid on the obstacle cause a high pressure field on that region. Figures 3.24 and 3.25 show mass conservation for both cases, with and without obstacle, respectively.



$t = 0$ $t = 0.7$ $t = 1.4$

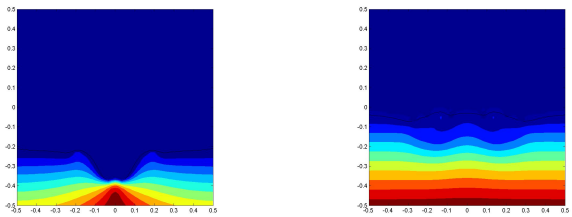


$t = 1.7$ $t = 1.775$ $t = 1.8$



$t = 1.9$ $t = 2.1$ $t = 2.5$

Figure 3.18. Bursting Bubble without jet formation in the presence of surface tension, $Eo = 300$.



(a) (b)

Figure 3.19. Pressure distribution at the moment of beginning of jet formation : a) Bubble is close to free surface. b) Bubble is far from free surface.

Since interface deformations are more tense in Dam Breaking problem rather than previous test cases, loss of mass conservation is increased. As it is obvious from Figure 3.25 mass loss becomes more severe after the time in which fluid hits the obstacle.

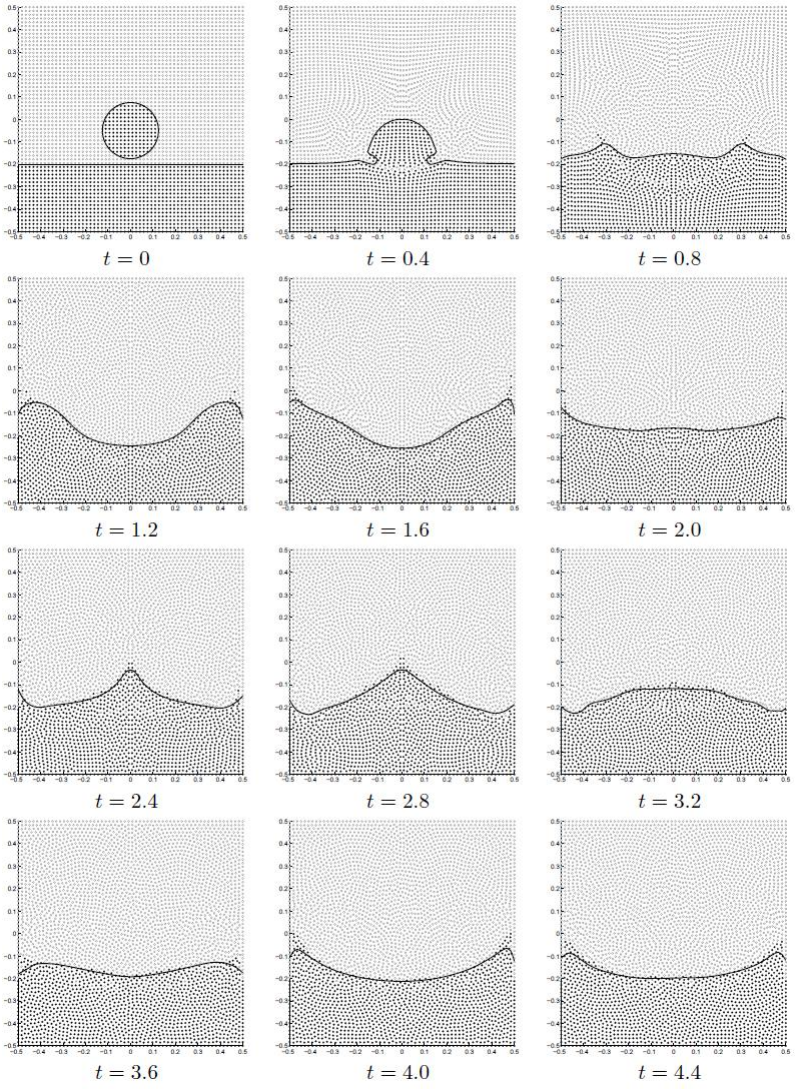
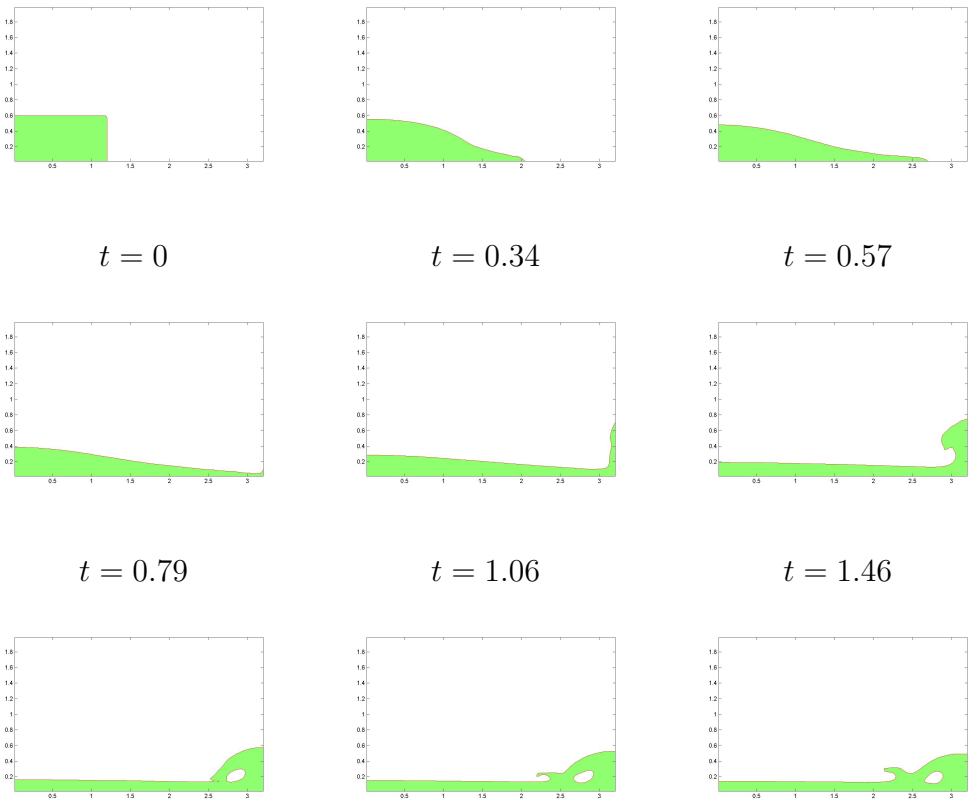


Figure 3.20. Droplet Fall onto a Free Surface: — represent Level Set Function, ● represents high density particles and ○ represents low density particles.

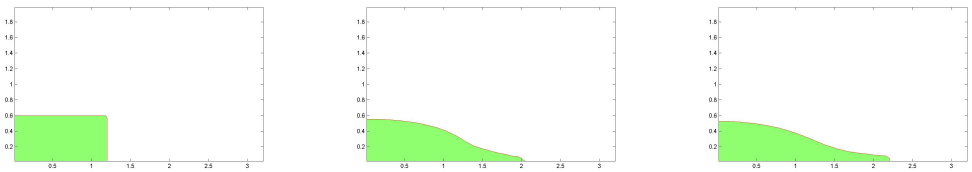


$t = 0$ $t = 0.34$ $t = 0.57$

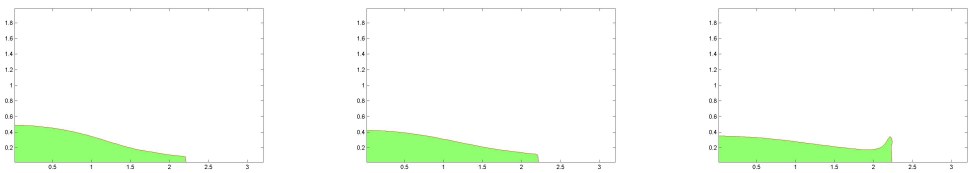
$t = 0.79$ $t = 1.06$ $t = 1.46$

$t = 1.66$ $t = 1.75$ $t = 1.84$

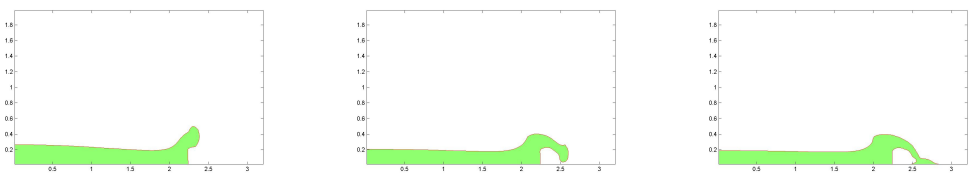
Figure 3.21. Dam Breaking without obstacle.



$t = 0$ $t = 0.34$ $t = 0.44$

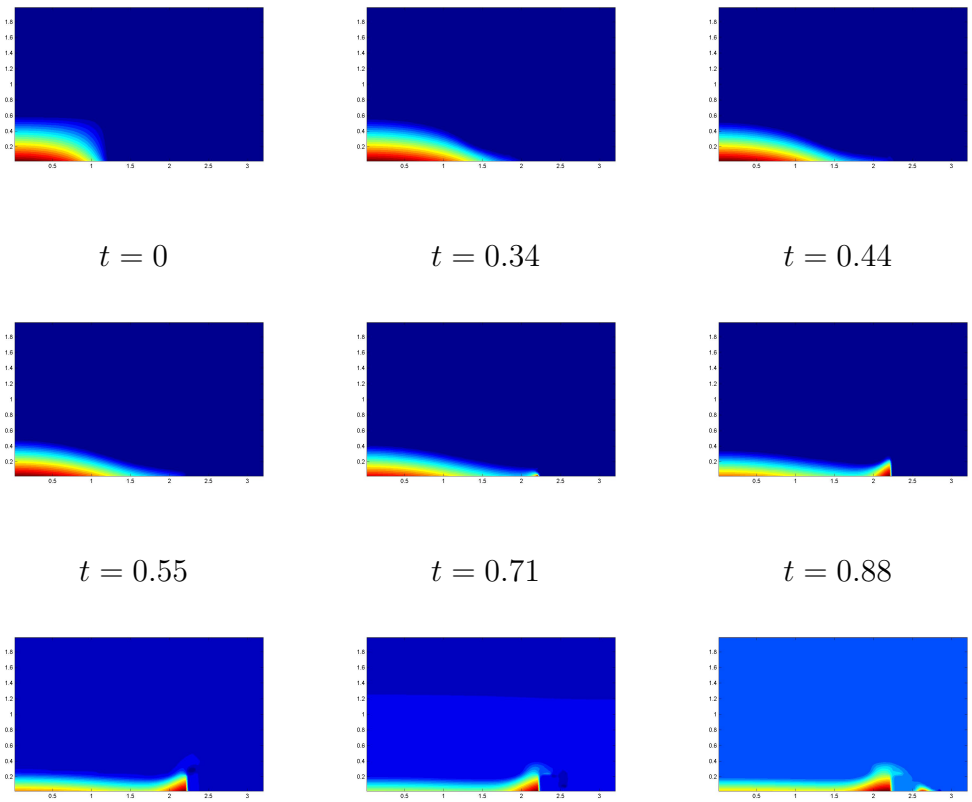


$t = 0.55$ $t = 0.71$ $t = 0.88$



$t = 1.13$ $t = 1.37$ $t = 1.48$

Figure 3.22. Dam Breaking with obstacle.



$t = 0$ $t = 0.34$ $t = 0.44$

$t = 0.55$ $t = 0.71$ $t = 0.88$

$t = 1.13$ $t = 1.37$ $t = 1.48$

Figure 3.23. Pressure Field for Dam Breaking with obstacle.

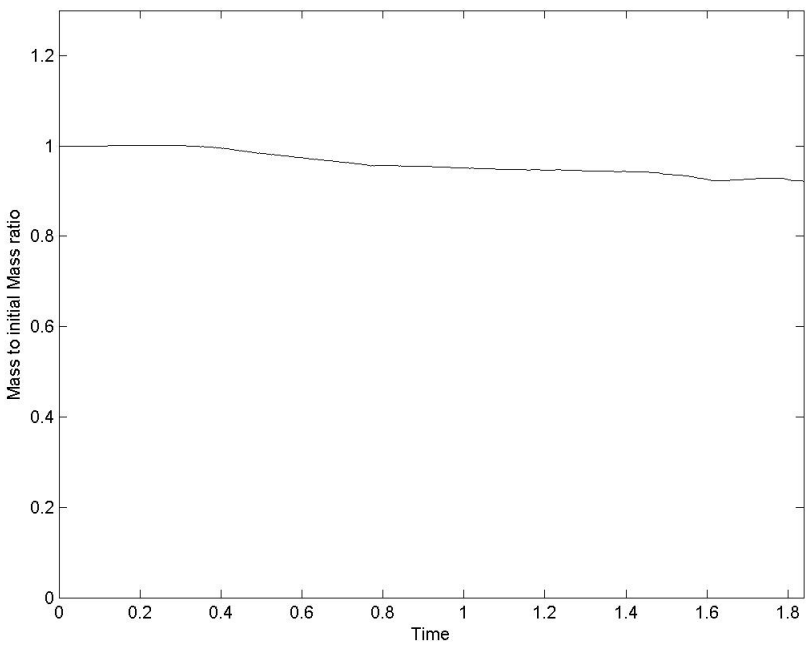


Figure 3.24. Mass conservation diagram for Dam Breaking without obstacle case.

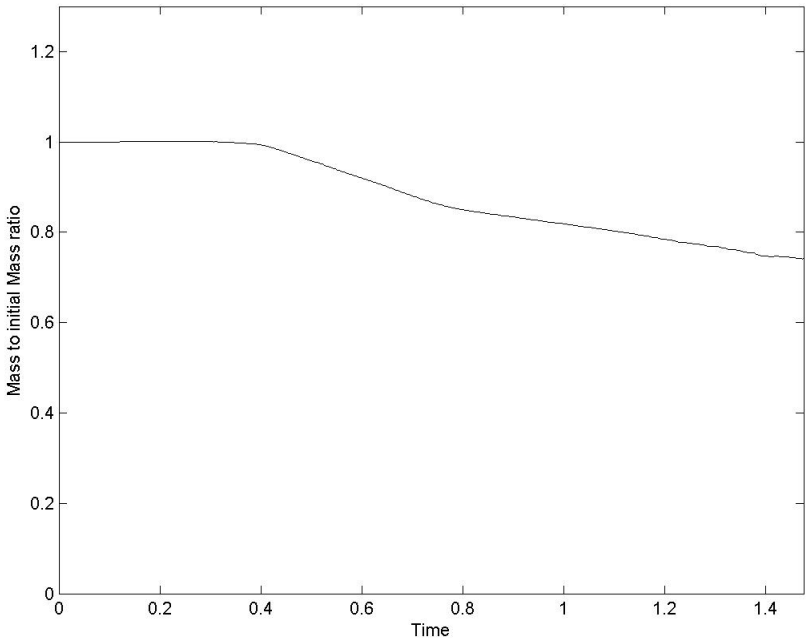


Figure 3.25. Mass conservation diagram for Dam Breaking with obstacle case.

4. CONCLUSIONS

In this study, Level Set method for handling two-phase interfacial flows is explained. Reliability of method is examined by making comparison with Smoothed Particle Hydrodynamics (SPH) method and good agreements are achieved. Well known test cases such as Rising Bubble, Rayleigh-Taylor instability, and Dam Breaking problems are considered in order to analyze behaviour of two-phase flows and effective parameters, surface tension coefficient (σ), Reynolds and Eotvos number, on such these flows.

It is seen that high surface tension (low Eotvos number) restricts bubble deformation in the surrounding fluid, i.e, in flows with high Eotvos number, bubble experiences more deformations. Surface tension force term may also affects the merging of two bubbles. If the surface tension is high enough, it may delay or even prevent the merging process. Moreover, high Reynolds number produces more intense circulations in the wake of bubble that may lead to seperation of bubble into smaller bubbles. One of the other effects of surface tension is in the formation of fluid jet after merging of bubble with the free surface. It is observed that in the presence of surface tension, the created fluid jet is shorter than in the case without surface tension. Note that initial distance between bubble and free surface is also effective in formation of fluid jet. If bubble is close enough to the free surface, high presseure difference that happen in a small region leads to jet formation.

Another test case in which surface tension is an effective parameter is Rayleigh-Taylor instability phenomenon. There is a critical value for surface tension in which the flow is stabilized. For surface tensions smaller than this critical value, grow of heavier fluid into the lighter one accelerates and Kelvin-Helmholtz instability happens more rapidly that results in more deformation of interface.

Although Level Set method shows a good performance in modeling two-phase flows and makes it easy to capture and follow the evolution of interface, mass conservation still remains as a significant problem especially in flows that interface experiences dramatically changes as seen in Dam Breaking test case. It is observed that mass reduction is severe at the moment fluid hits the wall or obstacle. Re-initialization procedures cure this problem to some extent, but it is not adequate. Coupling Level Set with methods that provide mass conservation such as VOF may be effective, but it spoils the simplicity of Level Set method. Using Adaptive Mesh Refinement (AMR) may be effective in order to apply denser mesh across the interface to increase the accuracy.

REFERENCES

1. Evans, M. and F. Harlow, *The Particle-in-Cell Method for Hydrodynamic Calculations*, Tech. rep., Los Alamos Scientific Laboratory., New Mexico., 1957.

2. Harlow, F. and J. Welch, "Numerical Calculation of Time-Dependent Viscous Incompressible Flow of Fluid with Free Surface", *Physics of Fluids*, Vol. 8, No. 12, p. 2182, 1965.

3. Harlow, F. and A. Amsden, "A Numerical Fluid Dynamics Calculation Method for all Flow Speeds", *Journal of Computational Physics*, Vol. 8, No. 2, pp. 197–213, 1971.

4. Glimm, J., X. Li, Y. Liu, Z. Xu and N. Zhao, "Conservative Front Tracking with Improved Accuracy", *SIAM Journal on Numerical Analysis*, pp. 1926–1947, 2004.

5. Moretti, G., "Computation of Flows with Shocks", *Annual Review of Fluid Mechanics*, Vol. 19, No. 1, pp. 313–337, 1987.

6. Peskin, C., "Numerical Analysis of Blood Flow in the Heart", *Journal of Computational Physics*, Vol. 25, No. 3, pp. 220–252, 1977.

7. Fauci, L. and C. Peskin, "A Computational Model of Aquatic Animal Locomotion", *Journal of Computational Physics*, Vol. 77, No. 1, pp. 85–108, 1988.

8. Fogelson, A. and C. Peskin, "A Fast Numerical Method for Solving the Three-Dimensional Stokes' Equations in the Presence of Suspended Particles", *Journal of Computational Physics*, Vol. 79, No. 1, pp. 50–69, 1988.

9. Tryggvason, G., B. Bunner, A. Esmaeeli, D. Juric, N. Al-Rawahi, W. Tauber, J. Han, S. Nas and Y. Jan, "A Front-Tracking Method for the Computations of Multiphase flow", *Journal of Computational Physics*, Vol. 169, No. 2, pp. 708–759,

2001.

10. Ervin, E. and G. Tryggvason, "The Rise of Bubbles in a Vertical Shear flow", *Journal of Fluids Engineering*, Vol. 119, p. 443, 1997.

11. Unverdi, S. and G. Tryggvason, "A Front-Tracking Method for Viscous, Incompressible, Multi-Fluid Flows", *Journal of Computational Physics*, Vol. 100, No. 1, pp. 25–37, 1992.

12. Lucy, L., "A Numerical Approach to the Testing of the Fission Hypothesis", *The Astronomical Journal*, Vol. 82, pp. 1013–1024, 1977.

13. Gingold, R. and J. Monaghan, "Smoothed Particle Hydrodynamics-Theory and Application to Non-Spherical Stars", *Monthly Notices of the Royal Astronomical Society*, Vol. 181, pp. 375–389, 1977.

14. Monaghan, J., "Simulating Free Surface Flows with SPH", *Journal of Computational Physics*, Vol. 110, pp. 399–399, 1994.

15. Cummins, S. and M. Rudman, "An SPH Projection Method", *Journal of Computational Physics*, Vol. 152, No. 2.

16. Hirt, C. and B. Nichols, "Volume of fluid (VOF) Method for the Dynamics of Free Boundaries", *Journal of Computational Physics*, Vol. 39, No. 1, pp. 201–225, 1981.

17. Noh, W. and P. Woodward, "SLIC (Simple Line Interface Calculation)", *Proceedings of the Fifth International Conference on Numerical Methods in Fluid Dynamics June 28–July 2, 1976 Twente University, Enschede*, pp. 330–340, Springer, 1976.

18. Youngs, D., "Time-Dependent Multi-Material Flow with Large Fluid Distortion", *Numerical Methods for Fluid Dynamics*, Vol. 24, pp. 273–285, 1982.

19. Scardovelli, R. and S. Zaleski, "Direct Numerical Simulation of Free-Surface and

Interfacial Flow", *Annual Review of Fluid Mechanics*, Vol. 31, No. 1, pp. 567–603, 1999.

20. Hohenberg, P. and B. Halperin, "Theory of Dynamic Critical Phenomena", *Reviews of Modern Physics*, Vol. 49, No. 3, p. 435, 1977.

21. Lowengrub, J. and L. Truskinovsky, "Quasi–Incompressible Cahn–Hilliard Fluids and Topological Transitions", *Proceedings of the Royal Society of London. Series A: Mathematical, Physical and Engineering Sciences*, Vol. 454, No. 1978, pp. 2617–2654, 1998.

22. Karma, A. and W. Rappel, "Quantitative Phase-Field Modeling of Dendritic Growth in Two and Three Dimensions", *Physical Review E*, Vol. 57, No. 4, p. 4323, 1998.

23. Osher, S. and J. Sethian, "Fronts Propagating with Curvature-Dependent Speed: Algorithms based on Hamilton-Jacobi Formulations", *Journal of Computational Physics*, Vol. 79, No. 1, pp. 12–49, 1988.

24. Sethian, J., *Level Set Methods and Fast Marching Methods: Evolving Interfaces in Computational Geometry, Fluid Mechanics, Computer Vision, and Materials Science*, 3, Cambridge Univ Pr, 1999.

25. Osher, S. and R. Fedkiw, *Level Set Methods and Dynamic Implicit Surfaces*, Vol. 153, Springer Verlag, 2003.

26. Malladi, R. and J. Sethian, "Image Processing via Level Set Curvature Flow", *Proceedings of the National Academy of Sciences*, Vol. 92, No. 15, p. 7046, 1995.

27. Chan, T. and L. Vese, "A Level Set Algorithm for Minimizing the Mumford-Shah Functional in Image Processing", *Variational and Level Set Methods in Computer Vision, 2001. Proceedings. IEEE Workshop on*, pp. 161–168, IEEE, 2001.

28. Malladi, R. and J. Sethian, "Image Processing via Level Set Curvature Flow", *Proceedings of the National Academy of Sciences*, Vol. 92, No. 15, p. 7046, 1995.

29. Gibou, F., R. Fedkiw, R. Caflisch and S. Osher, "A Level Set Approach for the Numerical Simulation of Dendritic Growth", *Journal of Scientific Computing*, Vol. 19, No. 1, pp. 183–199, 2003.

30. Chen, S., B. Merriman, S. Osher and P. Smereka, "A Simple Level Set Method for Solving Stefan Problems", *Journal of Computational Physics*, Vol. 135, No. 1, pp. 8–29, 1997.

31. Sethian, J. and J. Straint, "Crystal Growth and Dendritic Solidification", *Journal of Computational Physics*, Vol. 98, No. 2, pp. 231–253, 1992.

32. Sethian, J. and P. Smereka, "Level Set Methods for Fluid Interfaces", *Annual Review of Fluid Mechanics*, Vol. 35, No. 1, pp. 341–372, 2003.

33. Sussman, M., P. Smereka and S. Osher, *A Level Set Approach for Computing Solutions to Incompressible Two-Phase Flow*, Ph.D. Thesis, UCLA, 1994.

34. Sussman, M., A. Almgren, J. Bell, P. Colella, L. Howell and M. Welcome, "An Adaptive Level Set Approach for Incompressible Two-Phase Flows", *Journal of Computational Physics*, Vol. 148, No. 1, pp. 81–124, 1999.

35. Chang, Y., "A Level Set Formulation of Eulerian Interface Capturing Methods for Incompressible Fluid Flows", *Journal of Computational Physics*, Vol. 124, No. 2, pp. 449–464, 1996.

36. Peng, D., B. Merriman, S. Osher, H. Zhao and M. Kang, "A PDE-Based Fast Local Level Set Method", *Journal of Computational Physics*, Vol. 155, No. 2, pp. 410–438, 1999.

37. Jiang, G. and D. Peng, "Weighted ENO Schemes for Hamilton-Jacobi Equations",

SIAM Journal on Scientific Computing, Vol. 21, No. 6, pp. 2126–2143, 2000.

38. Croce, R., M. Griebel and M. Schweitzer, *A Parallel Level-Set Approach for Two-Phase Flow Problems with Surface Tension in Three Space Dimensions*, Citeseer, 2004.

39. Chorin, A., "Numerical Solution of the Navier-Stokes Equations", *Math. Comp*, Vol. 22, No. 104, pp. 745–762, 1968.

40. Saad, Y., R. I. for Advanced Computer Science (US) and A. R. Center, *Overview of Krylov Subspace Methods with Applications to Control Problems*, Research Institute for Advanced Computer Science, NASA Ames Research Center, 1989.

41. Huang, J. and H. Zhang, "Level Set Method for Numerical Simulation of a Cavitation Bubble, its Growth, Collapse and Rebound near a Rigid Wall", *Acta Mechanica Sinica*, Vol. 23, No. 6, pp. 645–653, 2007.

42. Gerya, T., *Introduction to Numerical Geodynamic Modelling*, Vol. 344, Cambridge University Press, 2010.

43. Ghia, U., K. Ghia and C. Shin, "High-Re Solutions for Incompressible Flow using the Navier-Stokes Equations and a Multigrid Method", *Journal of Computational Physics*, Vol. 48, No. 3, pp. 387–411, 1982.

44. Chandrasekhar, S., *Hydrodynamic and Hydromagnetic Stability*, Dover Pubns, 1961.